Spatially Resolved Temperature Response Functions to CO2 Emissions

Lyssa M Freese[1], Arlene M. Fiore[2], and Noelle Eckley Selin[1]

[1]Massachusetts Institute of Technology
[2]MIT

July 20, 2023

Abstract

The ability to rapidly simulate the climate implications of a large number of CO2 emissions trajectories is helpful for implementing mitigation and adaptation policies. A key variable of interest is near-surface air temperature, which is approximately proportional to cumulative CO2 emissions. We take advantage of this relationship, diagnosing Green's Functions for the spatial temperature response to CO2 emissions based on CMIP6 experiment data, creating an emulator that can be used across emissions scenarios to estimate local temperature responses. As compared to CMIP6 experiments, this approach captures the spatial temperature response with some limited accuracy in polar regions. It incorporates emissions path dependency and is useful for evaluating large ensembles of policy scenarios that are otherwise prohibitively expensive to simulate using earth system models. We apply this emulator to show differing local temperature responses when a global mean of 2ºC is reached and to varying trajectories with the same cumulative emissions.

Spatially Resolved Temperature Response Functions to CO_2 Emissions

Lyssa M. Freese [1], Arlene M. Fiore [1], Noelle E. Selin [1,2]

[1]Massachusetts Institute of Technology, Earth, Atmospheric, and Planetary Sciences
[2]Massachusetts Institute of Technology, Institute for Data, Systems, and Society

Key Points:

- With a Green's Function approach, we emulate the global mean and spatially resolved temperature response to a CO_2 emissions trajectory.
- This approach allows expedient emulation of the spatial and temporal temperature response to varying emissions pathways.
- We illustrate this approach by evaluating local temperatures when a global mean of 2°C is reached.

Corresponding author: Lyssa M. Freese, lyssamfreese@gmail.com

Corresponding author: Noelle E. Selin, selin@mit.edu

Abstract

The ability to rapidly simulate the climate implications of a large number of CO_2 emissions trajectories is helpful for implementing mitigation and adaptation policies. A key variable of interest is near-surface air temperature, which is approximately proportional to cumulative CO_2 emissions. We take advantage of this relationship, diagnosing Green's Functions for the spatial temperature response to CO_2 emissions based on CMIP6 experiment data, creating an emulator that can be used across emissions scenarios to estimate local temperature responses. As compared to CMIP6 experiments, this approach captures the spatial temperature response with some limited accuracy in polar regions. It incorporates emissions path dependency and is useful for evaluating large ensembles of policy scenarios that are otherwise prohibitively expensive to simulate using earth system models. We apply this emulator to show differing local temperature responses when a global mean of 2°C is reached and to varying trajectories with the same cumulative emissions.

Plain Language Summary

There is a wide range of potential pathways for future CO_2 emissions, and simulating them in earth system models can take large computational resources. It is important to understand the varying local impacts of different policies for effective mitigation and adaptation to climate change. A key concern is understanding local changes in temperature where people live. It is well established that the global mean temperature change is proportional to the cumulative emissions of CO_2; taking advantage of this relationship, we create a simplified model that quantifies local temperature response to CO_2 emissions. As it takes less than one second to emulate 90 years of temperature change, this approach can be used to evaluate a multitude of policy scenarios. We evaluate this approach with the Climate Model Intercomparison Project Phase 6 (CMIP6) experiment data, showing that it captures the temperature response in different locations with some limited accuracy in polar regions. We apply this approach to show local temperature change when a global mean temperature reaches 2°C.

1 Introduction

Evaluating uncertainty in coupled earth-society systems is important for understanding the impact of decision-making on society, and for developing metrics such as the social cost of carbon (SCC) (Interagency Working Group on Social Cost of Greenhouse Gases, United States Government, 2021; Carleton et al., 2022). One aspect of such uncertainty analysis involves evaluating the impacts of emissions trajectories from large ensembles of social scenarios to quantify impacts on the climate system. Because of the computational cost of running full-scale earth-system models, researchers rarely use them to evaluate large numbers of different emission scenarios. Detailed information drawn from these models, however, is useful for understanding the local climate impacts of decisions.

Current methods to evaluate the temperature response of the earth system to anthropogenic emissions of CO_2 include running global climate models (GCMs), earth system models (ESMs), earth system models of intermediate complexity (EMICs) (Claussen et al., 2002), energy balance models (EBMs) or multi-box models that underlie many integrated assessment models (IAMs). There is a tradeoff between model complexity (and thus the detail of results) and computational cost for all of these approaches. GCMs and ESMs are too computationally expensive to run large ensembles of policy scenarios. EMICs can evaluate the spatial temperature response to CO_2 emissions, with smaller computational costs due to lower resolution and reduced complexity physics. EBMs are computationally inexpensive, but provide only global mean or zonally-integrated representations of temperature changes.

The transient climate response to cumulative emissions of carbon dioxide (TCRE) (Matthews et al., 2009; Steinacher & Joos, 2016; Herrington & Zickfeld, 2014; Canadell et al., 2021) can be used to calculate the temperature impact of CO_2 emissions. Pattern scaling using the regional transient climate response to cumulative emissions of carbon dioxide (RTCRE) (Leduc et al., 2016) can provide low-cost, spatially explicit estimates of the temperature response to emissions. Applications of the RTCRE typically assume that the pattern response of temperature is constant and insensitive to the emissions trajectory, which can fail under varying emissions sizes and under reductions in emissions (Krasting et al., 2014; Zickfeld et al., 2016; Tokarska et al., 2019). This linearity and the TCRE have had important societal consequences, leading to the establishment of carbon budgets for a target global mean temperature (Meinshausen et al., 2009; Rogelj et al., 2011; Matthews et al., 2018; Matthews & Caldeira, 2008; Drake & Henderson, 2022).

Response operators, or Green's Functions, provide an alternate approach to diagnosing both global mean and spatial feedbacks to a forcing in ways that can capture differing pattern responses over time. Green's Functions have been used to characterize the radiative feedback response to sea surface temperature (Dong et al., 2019), temperature response to CO_2 concentrations (Lucarini et al., 2017; Lembo et al., 2020), and atmospheric transit times (Orbe et al., 2016). When diagnosed from ESMs, Green's Functions can form the basis for emulators that maintain the resolution of the original model, while reducing the computational load to simulate scenarios (as seen in Geoffroy and Saint-Martin (2014)).

Here, we construct an emulator, the Earth System Green's Response emulator (ESGR), of the pattern response of temperature to CO_2 emissions, which maintains the resolution of the ESMs it is derived from while enabling near-instantaneous computation. We take advantage of the approximately linear relationship between CO_2 emissions and temperature by diagnosing Green's Functions for temperature response to CO_2 emissions, using the Carbon Dioxide Removal Model Intercomparison Project (CDRMIP) model output (Keller et al., 2018). ESGR is based on the multi-model mean spatial Green's Function, and is evaluated with CMIP6 experiments. We show that it reproduces the temperature response due to emissions of CO_2 in most locations within one standard deviation of the CMIP6 multi-model mean both when CO_2 emissions are increasing and after their cessation. ESGR captures the time-dependent spatial patterns of the temperature response under two scenarios that end with the same cumulative CO_2 emissions. We illustrate how ESGR can be used to efficiently calculate metrics such as local temperature changes when a global mean 2 °C is reached.

2 Methods

We use model output from CDRMIP to build ESGR from calculated temperature responses to CO_2 emissions. Here we present the model data that is used to diagnose the Green's Functions and for evaluation, and explain the derivation and evaluation of ESGR.

2.1 CMIP6 Models

The Earth System Grid Federation (ESGF) archive includes six models that ran 250 years of pre-industrial control simulations (*esm-pi-ctrl*), as well as 100 gigaton carbon (GtC) pulse (*esm-pi-CO2pulse*) and removal (*esm-pi-CDRpulse*) emission simulations that branch from the *esm-pi-ctrl* at year 100 and allow the coupled carbon-climate system to respond over 90-140 years (Keller et al., 2018). There are six models with data from these experiments (shown in Table S1), each with two pulse scenarios (CanESM5 has 3 realizations of the pulse) for a total of 16 model runs. We compare ESGR to the difference between the *1pctCO*$_2$ or *esm-1pct-brch-1000PgC* experiment and the *esm-pi-ctrl* simulation for the same model source IDs as used to diagnose the Green's Function for evaluation (excluding GFDL as the data is unavaialable; see Table S2 for model information).

2.2 Spatial Green's Functions

We diagnose Green's Functions to create a spatiotemporally resolved pattern of temperature response to a CO_2 emissions pulse. In the case of CMIP6 experiment output, the change in the response variable of interest, T (near-surface air temperature at a location x), over time, is defined as:

$$\frac{\partial T(\mathbf{x})}{\partial t} = \mathcal{A}(T(\mathbf{x})) + E(t), \tag{1}$$

where $E(t)$ is the emissions forcing, and $\mathcal{A}(T)$ are the temperature tendency terms (everything impacting temperature aside from emissions, such as advection and radiation). Assuming that $\mathcal{A}(T)$ is independent of time and linear, we define a linear operator, $\mathcal{L} \equiv \frac{\partial}{\partial t} - \mathcal{A}$, that satisfies:

$$\mathcal{L}T(\mathbf{x}) = E(t). \tag{2}$$

A Green's Function, $G(\mathbf{x}, t-t')$, is defined as the response at location $\mathbf{x}$ and time t to an impulse (delta function) forcing at time $t = t'$ that satisfies the linear equation:

$$\mathcal{L}G(\mathbf{x}, t-t') = \delta(t-t'), \tag{3}$$

If we scale this by $E(t')$, and then integrate this over time, the resulting equation becomes:

$$\int \mathcal{L}G(\mathbf{x}, t-t')E(t')dt' = \int E(t')\delta(t-t')dt'. \tag{4}$$

Taking advantage of the assumed time-independence of $\mathcal{L}$, and that $\delta(t-t')$ is zero everywhere except where $t = t'$, we can simplify this as:

$$\mathcal{L}\left[\int G(\mathbf{x}, t-t')E(t')dt'\right] = E(t). \tag{5}$$

This takes the same form as 2, allowing us to equate

$$T(\mathbf{x}, t) = \int G(\mathbf{x}, t-t')E(t')dt', \tag{6}$$

providing a simple equation by which we can estimate the near-surface air temperature response given an emissions time series.

2.3 Diagnosing the Green's Functions from CMIP6

We can take this general form of the Green's Function and apply it to the CMIP6 pulse experiments. Here, $T_p(\mathbf{x}, t; t_0)$ is the temperature change due to either the *esm-pi-CO2pulse* or *esm-pi-CDRpulse* experiments relative to the *pi-ctrl*, and E_0 is the magnitude of the forcing from that pulse (100 or -100 GtC, respectively) at time t_0, resulting in:

$$\mathcal{L}T_p = E_0\delta(t-t_0). \tag{7}$$

Dividing equation 7 by the constant E_0, and using equation 3 we diagnose the Green's Function

$$G(\mathbf{x}, t - t_0) = \frac{T_p(\mathbf{x}, t; t_0)}{E_0}. \tag{8}$$

Assuming that G does not depend on the absolute time of the pulse, we can relabel the specific time t_0 to any time t', allowing us to convolve the Green's Function that is diagnosed in equation 8 with a forcing $E(t')$ at any time, as long as the scenario remains within present CO_2 states with up to 5000 GtC of cumulative emissions (as the linear relationship has been determined to hold to this level (Tokarska et al., 2016)).

Practically, we construct ESGR as the multi-model mean Green's Function for every grid box of the CMIP6 model output, equally weighting by model source ID. We use a 4th-order polynomial fit of the Green's Function to reduce the role of unforced internal variability (see Supplementary Information for an evaluation of unforced internal variability). In order to evaluate temperature response to a given emissions scenario, we convolve ESGR with emissions scenarios of CO_2 by summing the discretized integrands of equation 6 (using scipy's signal convolution (Virtanen et al., 2020)).

2.4 Evaluation

We evaluate ESGR with the *1pctCO*$_2$ and *esm-1pct-brch-1000PgC* experiments. The *1pctCO*$_2$ experiment prescribes a one percent increase in CO_2 concentration from pre-industrial conditions until four times the pre-industrial atmospheric concentration is reached (Eyring et al., 2016). The *esm-1pct-brch-1000PgC* experiment follows the *1pctCO*$_2$ experiment until 1000PgC has accumulated in the atmosphere after which it allows the carbon cycle to freely evolve with zero anthropogenic CO_2 emissions.

We calculate the underlying emissions profiles for these two experiments according to methods described in equation 2 of (Liddicoat et al., 2021), where the emissions have to balance the atmospheric CO_2 concentration (G_{ATM}), exchange with the ocean (S_{OCEAN}), and exchange with the land ($S_{LAND} - E_{LUC}$):

$$E_{CO_2} = G_{ATM} + S_{OCEAN} + (S_{LAND} - E_{LUC}) \tag{9}$$

Where (G_{ATM}) is the co2mass variable, exchange with the ocean (S_{ocean}) is fgco2, and exchange with the land ($S_{land} - E_{LUC}$) is nbp, all globally integrated.

The evaluation is performed by 1) convolving individual model Green's Functions with the corresponding diagnosed *1pctCO*$_2$ and *esm-1pct-brch-1000PgC* emissions profile, and 2) taking the weighted multi-model mean temperature response (weights are shown in Table S2). We convolve ESGR for each model ID and instance with the corresponding emissions and take the mean. ESGR depends in part on carbon cycle dynamics, so it has a non-zero correlation with the emissions that underlie an individual model's fixed CO_2 concentration experiments, and as a result, taking the mean before and after the convolution yield differing results. This is only necessary in the evaluation as emissions scenarios we independently create are not correlated to an individual model's response and can be convolved with the ESGR multi-model mean. We compare the ESGR near-surface air temperature response at every grid box with the weighted multi-model mean temperature difference between the *1pctCO*$_2$ or the *esm-1pct-brch-1000PgC* experiment and the *pi-ctrl* run.

2.5 Smoothing approach for the Green's Function

We reduce the role of unforced internal variability by taking the mean across multiple models (Lehner & Deser, 2023), and by using a 4th-order polynomial fit (Lehner & Deser, 2023; Hawkins & Sutton, 2009) to the Green's Function (see Supplementary

Information and Figure S6 for a comparison of different fits to the Green's Function). The convolution also smooths out much of the high-frequency variability that is introduced in the Green's function approach (see Supplementary Information and Figure S8 for a discussion of the Fourier transform of the Green's function, which shows the reduction of this noise).

2.6 Transient Climate Response, Zero Emissions Commitment, and Pattern Scaling Calculations

We calculate a TCR for each model source ID using the temperature response of a *1pctCO*$_2$ experiment at a doubling of CO_2, defined as the mean between years 60 and 80 following the method of Matthews et al. (2009). The TCRE is the TCR divided by the cumulative emissions to year 70 in a *1pctCO*$_2$ experiment (Matthews et al., 2009). We use an approach similar to that of (MacDougall et al., 2020) for the ZEC, taking the twenty-year global mean temperature anomaly centered 15 years after cessation of emissions.

In order to pattern scale the TCRE, we multiply it by the cumulative emissions at every time (based on Leduc et al. (2016)'s RTCRE pattern scaling).

3 Results

We first present an evaluation of ESGR with respect to global mean and pattern response, comparing the temperature change to that of the multi-model mean CMIP6 for *1pctCO*$_2$ and *esm-1pctCO*$_2$*-brch-1000PgC* experiments. We then illustrate two potential applications, demonstrating how ESGR can be used for calculating the impact of varying emissions trajectories on warming, and show that we capture the dependence of the final state of surface temperature change on not only the cumulative emissions but also the time-dependent emissions pathway. Importantly, this emulator takes under one second to simulate 90 years of temperature response, which allows for the evaluation of a multitude of emissions trajectories.

3.1 Evaluation: Global Mean Response

Figure 1a shows that the global mean time series of ESGR is positive, and has a time mean value of 1.49°C/1000GtC, reflecting the expected warming response to emissions of CO_2. All of the individual model Green's Functions have a positive time-mean value over time, which is again expected given the positive temperature response to increased CO_2 emissions. ESGR reproduces the global mean temperature response over time to the *1pctCO*$_2$ and the *esm-1pctCO*$_2$*-brch-1000PgC* experiments (Figure 1b). It captures both the positive increase in temperature as a response to increasing CO_2 emissions, and the cessation of warming when emissions are stopped under *esm-1pctCO*$_2$*-brch-1000PgC*.

We quantify ESGR's ability to reproduce the global mean temperature change through calculating the TCR and ZEC for both the ESGR and CMIP6 experiments (Figure 1c and d). The multi-model mean TCR, which indicates the global mean warming after a doubling of CO_2, is 2.12°C for the CMIP6 *1pctCO*$_2$ experiments, and ESGR has a TCR of 2.04°C. The inter-model spread of ESGR, particularly the minimum and maximum, cover a larger range than in the CMIP6 experiments, due to the variability in ESGR's ability to capture global mean temperature response for individual models. The global mean ZEC for ESGR is -0.028, indicating a slight decrease in temperature after a cessation of emissions. This mean response falls within the inter-quartile range (IQR) of the CMIP6 experiments' ZEC; however, the mean CMIP6 ZEC indicates continued warming with a ZEC of 0.088.

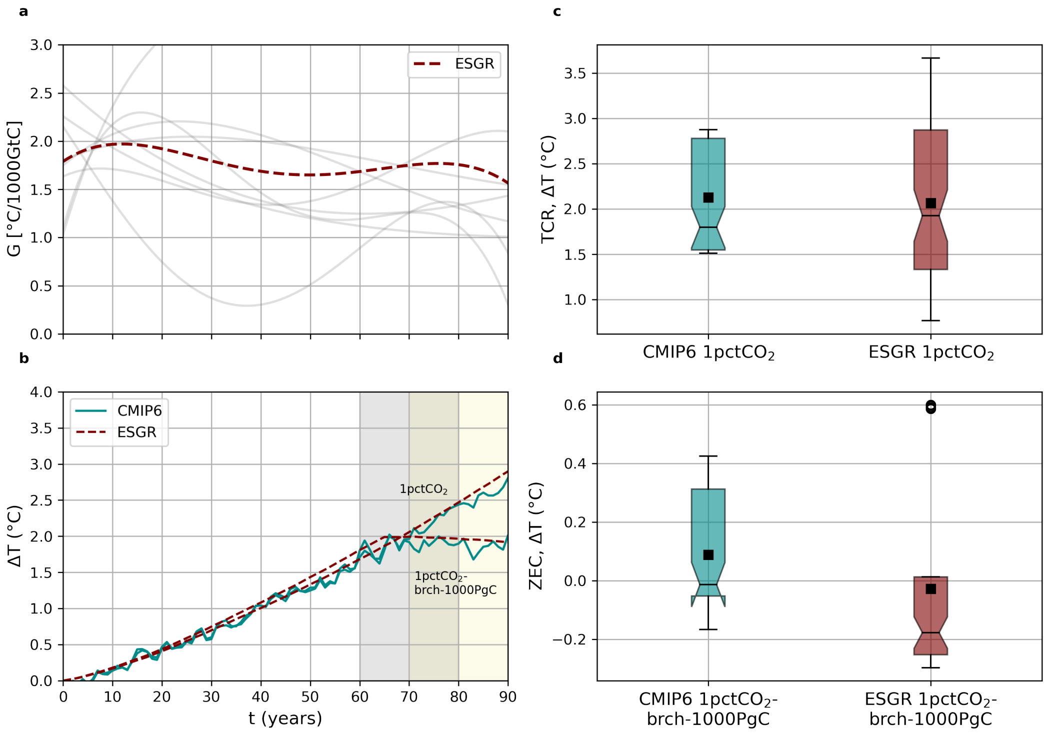

Figure 1. a) Global mean ESGR, and the spread of individual model Green's Functions. b) Mean of the *1pctCO*$_2$ and *esm-1pctCO*$_2$*-brch-1000PgC* emissions convolved with ESGR as compared to the multi-model mean of the *1pctCO*$_2$ and and *esm-1pctCO*$_2$*-brch-1000PgC* model runs compared to the *pi-ctrl*. Grey shading indicates the 20-year averaging period to calculate the TCR, and yellow shading indicates the 20-year time averaging period to calculate the ZEC. c and d) Mean, median, and interquartile range (IQR) of the TCR and ZEC (respectively).

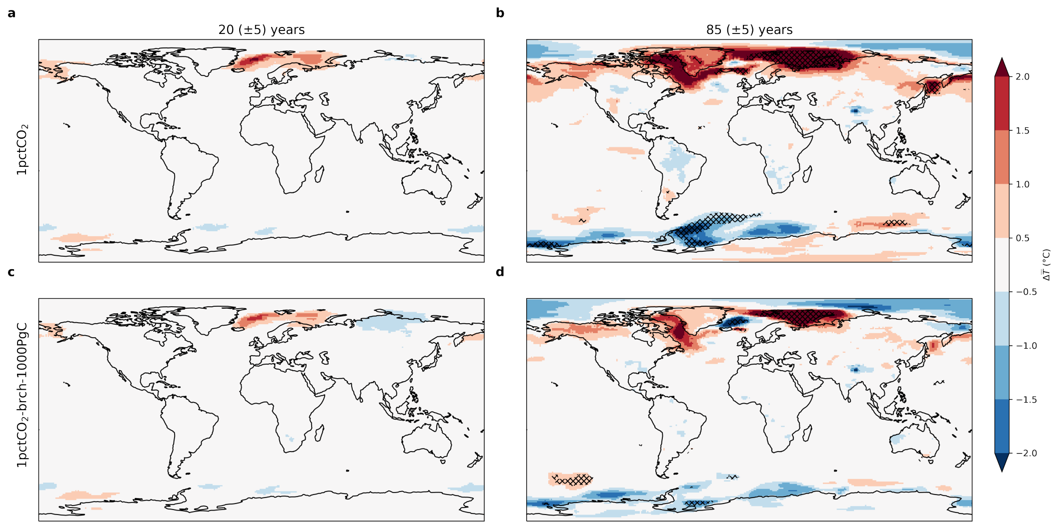

Figure 2. Difference in temperature response between ESGR *1pctCO*$_2$ (top) or ESGR *esm-1pct-brch-1000PgC* (bottom) and the multi-model mean CMIP6 *1pctCO*$_2$ or *esm-1pct-brch-1000PgC* experiment at 20($\pm$5) and 85($\pm$5) years. Hatching indicates locations that fall outside of a 1σ range of the model variability for the CMIP6 1pct model runs.

3.2 Evaluation: Pattern Response

Figure 2 shows the difference between the pattern response of ESGR and the multi-model mean CMIP6 *1pctCO*$_2$ and *esm-1pctCO*$_2$*-brch-1000PgC* experiments at 20 ($\pm$5) and 85 ($\pm$5) years. ESGR is able to capture the temperature response to both *1pctCO*$_2$ and *esm-1pctCO*$_2$*-brch-1000PgC* emissions over the first decade within 0.5°C of the CMIP6 model everywhere but the North Atlantic. After 20 years ESGR falls within one standard deviation of the CMIP6 model spread (Figure S5 shows the one standard deviation range), which we interpret as indicating the emulator is projecting a response consistent with the CMIP6 models. Over longer time periods, such as 85 years, ESGR is still able to capture the temperature response within 0.5°C of the CMIP6 experiments in all areas except for the Arctic and Antarctic due to nonlinearities from climate feedbacks (explored more in the Discussion and Conclusion). Even in the Arctic and Antarctic, many of the regions still fall within one standard deviation of the multi-model spread of CMIP6 responses; regions that are hatched are those that fall outside of this range. The temperature response in regions within one standard deviation of the multi-model mean CMIP6 responses are within the range of temperature responses that we would expect from an individual ESM. ESGR captures the reduced warming in year 85 of *esm-1pctCO*$_2$*-brch-1000PgC* as compared to the *1pctCO*$_2$, indicating that it can represent temperature response to both an increase and decrease in emissions (see Figure S4).

3.3 Application: Path-dependent Emissions Trajectories

ESGR can be used to show how emissions trajectories differ in their spatial temperature impact over time; here we calculate the outcomes of two example emissions scenarios that result in the same cumulative emissions. Trajectory 1 represents an increase in CO_2 emissions to 70 GtC/year over 20 years, followed by a rapid decline to zero GtC/year over 7 years, and Trajectory 2 represents an increase in CO_2 emissions to 37 GtC/year over 20 years, followed by a slow decline to zero GtC/year over 30 years. Both trajectories have the same cumulative emissions of 1050 GtC over a 120-year time span (Figure 3a). We convolve ESGR with these two trajectories creating *ESGR Traj 1* and *ESGR*

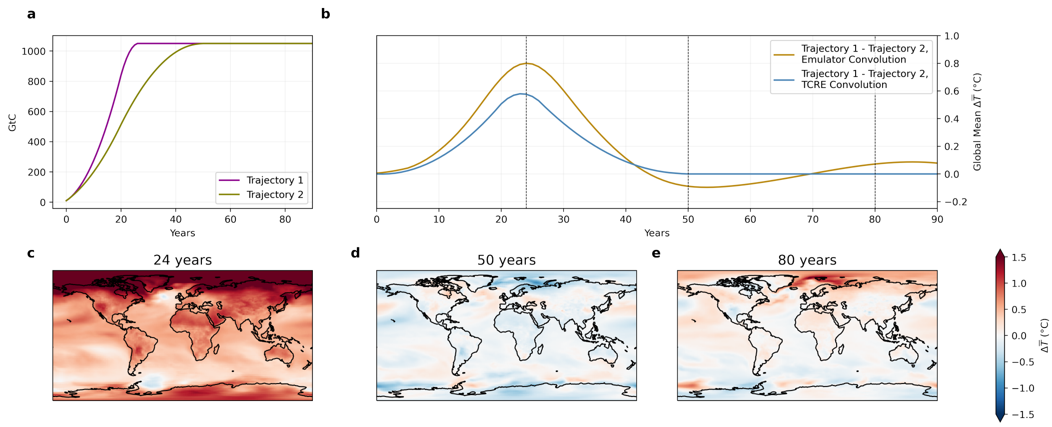

Figure 3. a) Cumulative emissions of CO_2 in GtC for 120 years in Trajectories 1 and 2. b) Global mean difference in temperature response to trajectories 1 and 2 convolved with either our Green's Function emulator or the TCRE. Dashed lines indicate years 24, 50, and 80 which are used in part c. c) The spatial pattern of the 10-year mean temperature difference between trajectories 1 and 2 convolved with our Green's Function emulator at years 24, 50, and 80 (all $\pm$ 5 years). The spatial pattern of temperature response by scaling the TCRE would have the same pattern of response throughout.

Traj 2. Figure 3 shows that at year 24, when the difference in cumulative emissions between the two scenarios is the greatest, there is more warming (both spatially and in the global mean) in *ESGR Traj 1* than *ESGR Traj 2*.

The calculated temperature response using ESGR is different than what results from scaling the TCRE by the cumulative emissions over time (as calculated in the Methods). This is expected, as the TCRE does not capture temperature responses when zero emissions are reached (Rogelj et al., 2018). Figure 3b shows that the peak temperature difference between Trajectories 1 and 2 is larger in ESGR than in a TCRE scaling, but the global mean temperature response does have a similar shape, as they both have peak differences in year 24. Once the two trajectories reach constant cumulative emissions, their global mean temperature in the TCRE convolution are, by definition, identical. However, there are fluctuations in the difference between *ESGR Traj 1* and *ESGR Traj 2* both in the global mean and spatially, capturing the emissions path dependency of warming (Krasting et al., 2014).

3.4 Application: Reaching Two Degrees of Warming

ESGR allows us to rapidly calculate the range of temperature response at different locations when a global mean temperature target is met under various emissions trajectories. We use the *1pctCO*$_2$ and 6 additional trajectories (see Supplementary Information) that ramp up emissions more slowly but that reach the same cumulative emissions as 1pctCO2 has when the global mean temperature response is 2°C to show the local temperature dependence on historical emissions pathways. In ESGR *1pctCO*$_2$, when a 2°C global mean is reached after 69 years, Boston, Shanghai, Buenos Aires, and Lagos are at decadal mean temperatures of 2.68°C, 2.35°C, 1.66°C, and 1.77°C, respectively. Under scenarios that reach the same cumulative emissions by year 69, however, the decadal mean local temperatures could range between 1.49°-2.68 °C (Boston), 1.46°-2.35 °C (Shanghai), 0.90°-1.66 °C (Buenos Aires), and 1.03°-1.77 °C (Lagos). The variation in final temperature shows the dependency of local temperature on the trajectory of emissions. These

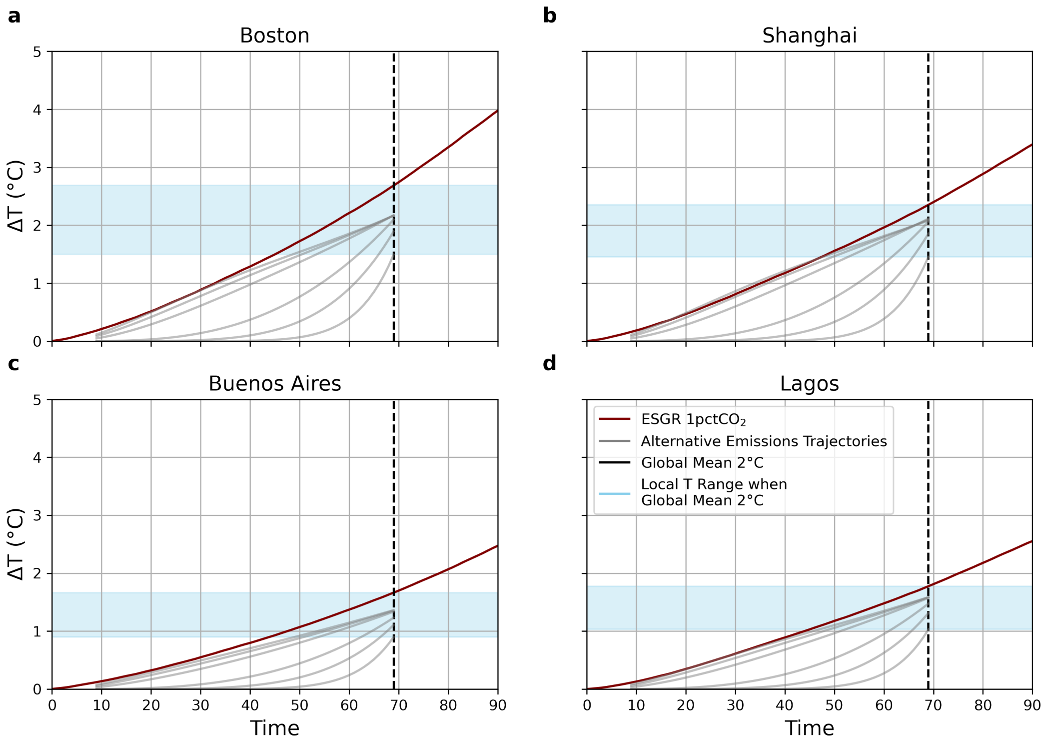

Figure 4. The time at which Boston, Shanghai, Buenos Aires, and Lagos reach 2 °C of warming. Black dashed lines show when the global mean temperature reaches 2°C. Horizontal blue shading indicates the local temperature range across our scenarios when a global mean of 2°C is reached. The emulated *1pctCO$_2$* response is in maroon and light grey lines show the alternative scenarios that reach the same cumulative emissions (all shown as a ten year mean).

results would be strongly sensitive to the use of a scaling approach (such as pattern scaling the RTCRE), as a pattern scaling would yield the exact same temperature response in each location under the different emissions trajectories.

4 Discussion and Conclusions

Understanding the relationship between global emissions and local impacts is necessary for evaluating emissions trajectories under uncertainty, mitigating climate change, and adapting to a warming world. Here, we establish a Green's Function emulator (ESGR) for spatially resolved temperature responses to cumulative global CO_2 emissions. ESGR allows users to rapidly assess the local responses to policy options and their resulting global CO_2 emissions trajectories. We evaluate this approach, which builds on the linear relationships between cumulative emissions and temperature change, by identifying where it falls within the model spread of ESM's. We apply ESGR to two emissions trajectories and use it to examine the local temperature response when the global mean reaches 2°C under multiple scenarios.

ESGR captures the global and local temperature response to both increases and reductions in CO_2 emissions, suggesting that it reproduces the different timescales of the radiative and carbon cycle responses. It does worst at estimating temperature response at high latitudes, overestimating temperature changes in the Arctic, and underestimating temperature changes in the Southern Ocean. Arctic amplification is the higher rate of warming that is experienced in the Arctic (Pierrehumbert, 2010; Manabe & Wetherald, 1975; Budyko, 1969; Previdi et al., 2021; Henry et al., 2021). Our overestimate in the Arctic (Figure S3), indicates that in the process of linearizing the response of the climate system, we overestimate the positive feedbacks that would occur due to emissions of an additional unit of CO_2, or that unforced internal variability is captured in this approach. The Southern Ocean is understood to have delayed warming due to the overturning circulation and the transport of warm waters northward (Armour et al., 2016). We either overestimate the negative feedbacks that would occur due to the emissions of an additional unit of CO_2, or incorporate unforced internal variability that leads to this delayed warming, leading to an incorporation of too much Southern Ocean delayed warming. Although ESGR could include unforced internal variability due to a mismatch in variability between the *pi-ctrl* and *esm-pi-CO2pulse*/*esm-pi-CDRpulse* experiments, we take multiple approaches to reduce the impact of this noise (see Supplementary Information).

ESGR can be applied to rapidly calculate metrics that can explore the implications of path dependence of local temperature response to CO_2. Previous work has shown the importance of emission pathways due to nonlinearities in the climate system, particularly when CO_2 emissions are reduced after overshoot scenarios (e.g. Zickfeld et al. (2016); Tokarska et al. (2019)). Here, we are able to reproduce the path dependence of the linear response of temperature to cumulative emissions (Krasting et al., 2014). One potential underlying reason for this is the balance between the different spatial patterns of the fast and slow components of global warming, where a reduction in CO_2 forcing leads to a fast exponential response on the order of magnitude of a few years, as well as a slow, recalcitrant response that leads to up to 50% of CO_2 being removed from the atmosphere within 30 years, equilibration with the ocean occurring on century timescales, and weathering occurring on millennial timescales (Held et al., 2010; Joos et al., 2013; Denman et al., 2007; Glotter et al., 2014). ESGR is able to reproduce these fast and slow responses; the pulse of CO_2 it is based on causes both immediate changes in atmospheric CO_2 concentration while still allowing for slow ocean carbon and heat uptake (Figure S3 shows variations in ESGR over time).

Many of the limitations of ESGR are due to experiments and data available from the CMIP6 archive, and based on this work we can evaluate what would be necessary to build on this approach. ESGR is built on Green's Functions derived from pulse emissions from a pre-industrial background state, and prior work has shown that atmospheric CO_2 concentration response is dependent on the background CO_2 concentration (Joos et al., 2013). This dependency is offset by the logarithmic relationship between CO_2 concentration and radiative forcing, leading to the linear response of temperature to CO_2 emissions (Caldeira & Kasting, 1993). Furthermore, work has shown that this linear relationship between CO_2 cumulative emissions and temperature holds at up to 5000 GtC of cumulative emissions in ESMs (Tokarska et al., 2016). Pulses of various sizes have been shown to influence the rate of the temperature response (Steinacher & Joos, 2016). However, the impact of emissions size is smaller than the impact of using various models (Krasting et al., 2014). As a result, the linear response function we derive here should be robust across varying background concentrations of CO_2 and emission sizes.

These assumptions could be better tested with additional ESM experiments to quantify the impact of pulse size, background state, short and long responses of the climate system, and internal variability. Additional ESM experiments pulsing varying sizes of emissions from a different starting condition would allow for quantification of the impact of the pulse size and background state– currently, the closest available experiments are the *CDR-yr2010-pulse* experiments, which are not publicly available on the Earth System Grid Federation (ESGF) and have been run in EMICs. If the pulse (*esm-pi-CO2pulse*) and removal (*esm-pi-CDRpulse*) experiments were run for longer time periods, this would improve our ability to evaluate long timescales and estimate variations in the ZEC over time (MacDougall et al., 2020). Lastly, an ensemble of pulse emissions from individual models would allow for better quantification of the role of internal variability, and for averaging out its impact on the Green's Function. As climate models improve, and as more become available, ESGR can be updated easily to reflect the latest state of the science.

Open Research Section

All code to reproduce this work is available on Zenodo (currently available on github at `https://github.com/lfreese/CO2_greens`, to be updated to Zenodo for publication). The raw data from CMIP6 is available at `https://esgf-node.llnl.gov/search/cmip6/`, and all of the experiments and runs used are described in Tables S1 and S2.

Acknowledgments

Author Contributions: Conceptualization: LF; Method development: LF; Analysis: LF; Interpretation: LF, NS, AF; Writing-original draft: LF; Writing-edits and review: LF, NS, AF; Supervision: NS.

We thank the NIEHS Toxicology Training Grant no. T32-ES007020 and the MIT Martin Family Society of Fellows for Sustainability (L.M.F.). This work was supported in part by the MIT Climate Grand Challenges project "Bringing Computation to the Climate Challenge" (L.M.F., N.E.S., and A.M.F.).

References

Armour, K. C., Marshall, J., Scott, J. R., Donohoe, A., & Newsom, E. R. (2016, July). Southern Ocean warming delayed by circumpolar upwelling and equatorward transport. *Nature Geoscience*, *9*(7), 549–554. Retrieved 2023-03-28, from `https://www.nature.com/articles/ngeo2731` (Number: 7 Publisher: Nature Publishing Group) doi: 10.1038/ngeo2731

Budyko, M. I. (1969, January). The effect of solar radiation variations on the climate of the Earth. , *21*(5), 611. Retrieved 2023-04-18, from `https://a.tellusjournals.se/articles/10.3402/tellusa.v21i5.10109` (Number: 5 Publisher: Stockholm University Press) doi: 10.3402/tellusa.v21i5.10109

Caldeira, K., & Kasting, J. F. (1993, November). Insensitivity of global warming potentials to carbon dioxide emission scenarios. *Nature*, *366*(6452), 251–253. Retrieved 2023-04-18, from `https://www.nature.com/articles/366251a0` (Number: 6452 Publisher: Nature Publishing Group) doi: 10.1038/366251a0

Canadell, J., Monteiro, P., Costa, M., da Cunha, L. C., Cox, P., Eliseev, A., ... Zickfeld, a. K. (2021). Global Carbon and other Biogeochemical Cycles and Feedbacks. *Climate Change 2021: The Physical Science Basis. Contribution of Working Group I to the Sixth Assessment Report of the Intergovernmental Panel on Climate Change*, 673–816. ([Masson-Delmotte, V., P. Zhai, A. Pirani, S.L. Connors, C. Péan, S. Berger, N. Caud, Y. Chen, L. Goldfarb, M.I. Gomis, M. Huang, K. Leitzell, E. Lonnoy, J.B.R. Matthews, T.K. Maycock, T. Waterfield, O. Yelekçi, R. Yu, and B. Zhou (eds.)]) doi: 10.1017/9781009157896.007

Carleton, T., Jina, A., Delgado, M., Greenstone, M., Houser, T., Hsiang, S., ... Zhang, A. T. (2022, November). Valuing the Global Mortality Consequences of Climate Change Accounting for Adaptation Costs and Benefits. *The Quarterly Journal of Economics*, *137*(4), 2037–2105. Retrieved 2022-12-09, from `https://doi.org/10.1093/qje/qjac020` doi: 10.1093/qje/qjac020

Claussen, M., Mysak, L., Weaver, A., Crucifix, M., Fichefet, T., Loutre, M.-F., ... Wang, Z. (2002, March). Earth system models of intermediate complexity: closing the gap in the spectrum of climate system models. *Climate Dynam-*

ics, *18*(7), 579–586. Retrieved 2023-03-29, from https://doi.org/10.1007/s00382-001-0200-1 doi: 10.1007/s00382-001-0200-1

Denman, K. L., Brasseur, G., Chidthaisong, A., Ciais, P., Cox, P. M., Dickinson, R. E., ... Molina, M. (2007). *Couplings Between Changes in the Climate System and Biogeochemistry* (Climate Change 2007: The Physical Science Basis). Cambridge University Press, Cambridge, United Kingdom and New York, NY, USA..

Dong, Y., Proistosescu, C., Armour, K., & Battisti, D. (2019). Attributing Historical and Future Evolution of Radiative Feedbacks to Regional Warming Patterns using a Green's Function Approach: The Preeminence of the Western Pacific. *Journal of Climate*, *Volume 32*(Issue 17). Retrieved 2022-07-08, from https://journals.ametsoc.org/view/journals/clim/32/17/jcli-d-18-0843.1.xml

Drake, H. F., & Henderson, G. (2022, May). A defense of usable climate mitigation science: how science can contribute to social movements. *Climatic Change*, *172*(1), 10. Retrieved 2022-11-25, from https://doi.org/10.1007/s10584-022-03347-6 doi: 10.1007/s10584-022-03347-6

Eyring, V., Bony, S., Meehl, G. A., Senior, C. A., Stevens, B., Stouffer, R. J., & Taylor, K. E. (2016, May). Overview of the Coupled Model Intercomparison Project Phase 6 (CMIP6) experimental design and organization. *Geoscientific Model Development*, *9*(5), 1937–1958. Retrieved 2023-03-13, from https://gmd.copernicus.org/articles/9/1937/2016/ (Publisher: Copernicus GmbH) doi: 10.5194/gmd-9-1937-2016

Geoffroy, O., & Saint-Martin, D. (2014, December). Pattern decomposition of the transient climate response. *Tellus A: Dynamic Meteorology and Oceanography*, *66*(1), 23393. Retrieved 2023-04-18, from https://a.tellusjournals.se/article/10.3402/tellusa.v66.23393/ doi: 10.3402/tellusa.v66.23393

Glotter, M. J., Pierrehumbert, R. T., Elliott, J. W., Matteson, N. J., & Moyer, E. J. (2014, October). A simple carbon cycle representation for economic and policy analyses. *Climatic Change*, *126*(3), 319–335. Retrieved 2023-04-18, from https://doi.org/10.1007/s10584-014-1224-y doi: 10.1007/s10584-014-1224-y

Hawkins, E., & Sutton, R. (2009, August). The Potential to Narrow Uncertainty in Regional Climate Predictions. *Bulletin of the American Meteorological Society*, *90*(8), 1095–1108. Retrieved 2023-05-30, from https://journals.ametsoc.org/view/journals/bams/90/8/2009bams2607_1.xml (Publisher: American Meteorological Society Section: Bulletin of the American Meteorological Society) doi: 10.1175/2009BAMS2607.1

Held, I. M., Winton, M., Takahashi, K., Delworth, T., Zeng, F., & Vallis, G. K. (2010, May). Probing the Fast and Slow Components of Global Warming by Returning Abruptly to Preindustrial Forcing. *Journal of Climate*, *23*(9), 2418–2427. Retrieved 2023-02-13, from https://journals.ametsoc.org/view/journals/clim/23/9/2009jcli3466.1.xml (Publisher: American Meteorological Society Section: Journal of Climate) doi: 10.1175/2009JCLI3466.1

Henry, M., Merlis, T. M., Lutsko, N. J., & Rose, B. E. J. (2021, March). Decomposing the Drivers of Polar Amplification with a Single-Column Model. *Journal of Climate*, *34*(6), 2355–2365. Retrieved 2023-04-24, from https://journals.ametsoc.org/view/journals/clim/34/6/JCLI-D-20-0178.1.xml (Publisher: American Meteorological Society Section: Journal of Climate) doi: 10.1175/JCLI-D-20-0178.1

Herrington, T., & Zickfeld, K. (2014, November). Path independence of climate and carbon cycle response over a broad range of cumulative carbon emissions. *Earth System Dynamics*, *5*(2), 409–422. Retrieved 2023-02-14, from https://esd.copernicus.org/articles/5/409/2014/ (Publisher: Copernicus GmbH) doi: 10.5194/esd-5-409-2014

Interagency Working Group on Social Cost of Greenhouse Gases, United States Government. (2021). *Technical Support Document: Social Cost of Carbon, Methane, and Nitrous Oxide.* Retrieved 2022-12-13, from https://web.archive.org/web/20221212061639/https://www.whitehouse.gov/wp-content/uploads/2021/02/TechnicalSupportDocument_SocialCostofCarbonMethaneNitrousOxide.pdf

Joos, F., Roth, R., Fuglestvedt, J. S., Peters, G. P., Enting, I. G., von Bloh, W., ... Weaver, A. J. (2013, March). Carbon dioxide and climate impulse response functions for the computation of greenhouse gas metrics: a multi-model analysis. *Atmospheric Chemistry and Physics*, *13*(5), 2793–2825. Retrieved 2020-12-16, from https://acp.copernicus.org/articles/13/2793/2013/ doi: 10.5194/acp-13-2793-2013

Keller, D. P., Lenton, A., Scott, V., Vaughan, N. E., Bauer, N., Ji, D., ... Zickfeld, K. (2018, March). The Carbon Dioxide Removal Model Intercomparison Project (CDRMIP): rationale and experimental protocol for CMIP6. *Geoscientific Model Development*, *11*(3), 1133–1160. Retrieved 2022-11-04, from https://gmd.copernicus.org/articles/11/1133/2018/ (Publisher: Copernicus GmbH) doi: 10.5194/gmd-11-1133-2018

Krasting, J. P., Dunne, J. P., Shevliakova, E., & Stouffer, R. J. (2014). Trajectory sensitivity of the transient climate response to cumulative carbon emissions. *Geophysical Research Letters*, *41*(7), 2520–2527. Retrieved 2023-03-29, from https://onlinelibrary.wiley.com/doi/abs/10.1002/2013GL059141 (_eprint: https://agupubs.onlinelibrary.wiley.com/doi/pdf/10.1002/2013GL059141) doi: 10.1002/2013GL059141

Leduc, M., Matthews, H. D., & de Elía, R. (2016, May). Regional estimates of the transient climate response to cumulative CO2 emissions. *Nature Climate Change*, *6*(5), 474–478. Retrieved 2023-01-30, from https://www.nature.com/articles/nclimate2913 (Number: 5 Publisher: Nature Publishing Group) doi: 10.1038/nclimate2913

Lehner, F., & Deser, C. (2023, May). Origin, importance, and predictive limits of internal climate variability. *Environmental Research: Climate*, *2*(2), 023001. Retrieved 2023-05-24, from https://dx.doi.org/10.1088/2752-5295/accf30 (Publisher: IOP Publishing) doi: 10.1088/2752-5295/accf30

Lembo, V., Lucarini, V., & Ragone, F. (2020, December). Beyond Forcing Scenarios: Predicting Climate Change through Response Operators in a Coupled General Circulation Model. *Scientific Reports*, *10*(1), 8668. Retrieved 2021-03-31, from http://www.nature.com/articles/s41598-020-65297-2 doi: 10.1038/s41598-020-65297-2

Liddicoat, S. K., Wiltshire, A. J., Jones, C. D., Arora, V. K., Brovkin, V., Cadule, P., ... Ziehn, T. (2021, April). Compatible Fossil Fuel CO2 Emissions in the CMIP6 Earth System Models' Historical and Shared Socioeconomic Pathway Experiments of the Twenty-First Century. *Journal of Climate*, *34*(8), 2853–2875. Retrieved 2022-11-04, from https://journals.ametsoc.org/view/journals/clim/34/8/JCLI-D-19-0991.1.xml (Publisher: American Meteorological Society Section: Journal of Climate) doi: 10.1175/JCLI-D-19-0991.1

Lucarini, V., Ragone, F., & Lunkeit, F. (2017, February). Predicting Climate Change Using Response Theory: Global Averages and Spatial Patterns. *Journal of Statistical Physics*, *166*(3-4), 1036–1064. Retrieved 2021-03-31, from http://link.springer.com/10.1007/s10955-016-1506-z doi: 10.1007/s10955-016-1506-z

MacDougall, A. H., Frölicher, T. L., Jones, C. D., Rogelj, J., Matthews, H. D., Zickfeld, K., ... Ziehn, T. (2020, June). Is there warming in the pipeline? A multi-model analysis of the Zero Emissions Commitment from CO_2. *Biogeosciences*, *17*(11), 2987–3016. Retrieved 2023-03-15, from https://

bg.copernicus.org/articles/17/2987/2020/ (Publisher: Copernicus GmbH) doi: 10.5194/bg-17-2987-2020

Manabe, S., & Wetherald, R. T. (1975, January). The Effects of Doubling the CO2 Concentration on the climate of a General Circulation Model. *Journal of the Atmospheric Sciences*, *32*(1), 3–15. Retrieved 2023-04-18, from https://journals.ametsoc.org/view/journals/atsc/32/1/1520-0469_1975_032_0003_teodtc_2_0_co_2.xml (Publisher: American Meteorological Society Section: Journal of the Atmospheric Sciences) doi: 10.1175/1520-0469(1975)032⟨0003:TEODTC⟩2.0.CO;2

Matthews, H. D., & Caldeira, K. (2008). Stabilizing climate requires near-zero emissions. *Geophysical Research Letters*, *35*(4). Retrieved 2022-11-04, from https://onlinelibrary.wiley.com/doi/abs/10.1029/2007GL032388 (_eprint: https://onlinelibrary.wiley.com/doi/pdf/10.1029/2007GL032388) doi: 10.1029/2007GL032388

Matthews, H. D., Gillett, N. P., Stott, P. A., & Zickfeld, K. (2009, June). The proportionality of global warming to cumulative carbon emissions. *Nature*, *459*(7248), 829–832. Retrieved 2022-11-04, from https://www.nature.com/articles/nature08047 (Number: 7248 Publisher: Nature Publishing Group) doi: 10.1038/nature08047

Matthews, H. D., Zickfeld, K., Knutti, R., & Allen, M. R. (2018, January). Focus on cumulative emissions, global carbon budgets and the implications for climate mitigation targets. *Environmental Research Letters*, *13*(1), 010201. Retrieved 2023-02-15, from https://dx.doi.org/10.1088/1748-9326/aa98c9 (Publisher: IOP Publishing) doi: 10.1088/1748-9326/aa98c9

Meinshausen, M., Meinshausen, N., Hare, W., Raper, S. C. B., Frieler, K., Knutti, R., ... Allen, M. R. (2009, April). Greenhouse-gas emission targets for limiting global warming to 2 °C. *Nature*, *458*(7242), 1158–1162. Retrieved 2023-04-18, from https://www.nature.com/articles/nature08017 (Number: 7242 Publisher: Nature Publishing Group) doi: 10.1038/nature08017

Orbe, C., Waugh, D. W., Newman, P. A., & Steenrod, S. (2016, October). The Transit-Time Distribution from the Northern Hemisphere Midlatitude Surface. *Journal of the Atmospheric Sciences*, *73*(10), 3785–3802. Retrieved 2022-07-12, from https://journals.ametsoc.org/view/journals/atsc/73/10/jas-d-15-0289.1.xml (Publisher: American Meteorological Society Section: Journal of the Atmospheric Sciences) doi: 10.1175/JAS-D-15-0289.1

Pierrehumbert, R. (2010). 4.4: Real gas radiation: basic principles. In *Principles of Planetary Climate.* New York: Cambridge University Press.

Previdi, M., Smith, K. L., & Polvani, L. M. (2021, September). Arctic amplification of climate change: a review of underlying mechanisms. *Environmental Research Letters*, *16*(9), 093003. Retrieved 2023-04-24, from https://dx.doi.org/10.1088/1748-9326/ac1c29 (Publisher: IOP Publishing) doi: 10.1088/1748-9326/ac1c29

Rogelj, J., Hare, W., Lowe, J., van Vuuren, D. P., Riahi, K., Matthews, B., ... Meinshausen, M. (2011, November). Emission pathways consistent with a 2 °C global temperature limit. *Nature Climate Change*, *1*(8), 413–418. Retrieved 2023-04-18, from https://www.nature.com/articles/nclimate1258 (Number: 8 Publisher: Nature Publishing Group) doi: 10.1038/nclimate1258

Rogelj, J., Shindell, D., Jiang, K., Fifita, S., Forster, P., Ginzburg, V., ... Vilariño, M. (2018). *Mitigation Pathways Compatible with 1.5°C in the Context of Sustainable Development. In: Global Warming of 1.5°C. An IPCC Special Report on the impacts of global warming of 1.5°C above pre-industrial levels and related global greenhouse gas emission pathways, in the context of strengthening the global response to the threat of climate change, sustainable development, and efforts to eradicate poverty.*

Steinacher, M., & Joos, F. (2016, February). Transient Earth system responses to cumulative carbon dioxide emissions: linearities, uncertainties, and probabilities in an observation-constrained model ensemble. *Biogeosciences*, *13*(4), 1071–1103. Retrieved 2023-02-14, from `https://bg.copernicus.org/articles/13/1071/2016/bg-13-1071-2016-discussion.html` (Publisher: Copernicus GmbH) doi: 10.5194/bg-13-1071-2016

Tokarska, K. B., Gillett, N. P., Weaver, A. J., Arora, V. K., & Eby, M. (2016, September). The climate response to five trillion tonnes of carbon. *Nature Climate Change*, *6*(9), 851–855. Retrieved 2023-03-09, from `https://www.nature.com/articles/nclimate3036` (Number: 9 Publisher: Nature Publishing Group) doi: 10.1038/nclimate3036

Tokarska, K. B., Zickfeld, K., & Rogelj, J. (2019). Path Independence of Carbon Budgets When Meeting a Stringent Global Mean Temperature Target After an Overshoot. *Earth's Future*, *7*(12), 1283–1295. Retrieved 2023-03-24, from `https://onlinelibrary.wiley.com/doi/abs/10.1029/2019EF001312` (_eprint: https://onlinelibrary.wiley.com/doi/pdf/10.1029/2019EF001312) doi: 10.1029/2019EF001312

Virtanen, P., Gommers, R., Oliphant, T. E., Haberland, M., Reddy, T., Cournapeau, D., ... van Mulbregt, P. (2020, March). SciPy 1.0: fundamental algorithms for scientific computing in Python. *Nature Methods*, *17*(3), 261–272. Retrieved 2022-11-04, from `https://www.nature.com/articles/s41592-019-0686-2` (Number: 3 Publisher: Nature Publishing Group) doi: 10.1038/s41592-019-0686-2

Zickfeld, K., MacDougall, A. H., & Matthews, H. D. (2016, May). On the proportionality between global temperature change and cumulative CO2 emissions during periods of net negative CO2 emissions. *Environmental Research Letters*, *11*(5), 055006. Retrieved 2023-03-24, from `https://dx.doi.org/10.1088/1748-9326/11/5/055006` (Publisher: IOP Publishing) doi: 10.1088/1748-9326/11/5/055006

Spatially Resolved Temperature Response Functions to CO_2 Emissions

Lyssa M. Freese [1], Arlene M. Fiore [1], Noelle E. Selin [1,2]

[1]Massachusetts Institute of Technology, Earth, Atmospheric, and Planetary Sciences
[2]Massachusetts Institute of Technology, Institute for Data, Systems, and Society

Key Points:

- With a Green's Function approach, we emulate the global mean and spatially resolved temperature response to a CO_2 emissions trajectory.
- This approach allows expedient emulation of the spatial and temporal temperature response to varying emissions pathways.
- We illustrate this approach by evaluating local temperatures when a global mean of 2°C is reached.

Corresponding author: Lyssa M. Freese, `lyssamfreese@gmail.com`

Corresponding author: Noelle E. Selin, `selin@mit.edu`

Abstract

The ability to rapidly simulate the climate implications of a large number of CO_2 emissions trajectories is helpful for implementing mitigation and adaptation policies. A key variable of interest is near-surface air temperature, which is approximately proportional to cumulative CO_2 emissions. We take advantage of this relationship, diagnosing Green's Functions for the spatial temperature response to CO_2 emissions based on CMIP6 experiment data, creating an emulator that can be used across emissions scenarios to estimate local temperature responses. As compared to CMIP6 experiments, this approach captures the spatial temperature response with some limited accuracy in polar regions. It incorporates emissions path dependency and is useful for evaluating large ensembles of policy scenarios that are otherwise prohibitively expensive to simulate using earth system models. We apply this emulator to show differing local temperature responses when a global mean of 2°C is reached and to varying trajectories with the same cumulative emissions.

Plain Language Summary

There is a wide range of potential pathways for future CO_2 emissions, and simulating them in earth system models can take large computational resources. It is important to understand the varying local impacts of different policies for effective mitigation and adaptation to climate change. A key concern is understanding local changes in temperature where people live. It is well established that the global mean temperature change is proportional to the cumulative emissions of CO_2; taking advantage of this relationship, we create a simplified model that quantifies local temperature response to CO_2 emissions. As it takes less than one second to emulate 90 years of temperature change, this approach can be used to evaluate a multitude of policy scenarios. We evaluate this approach with the Climate Model Intercomparison Project Phase 6 (CMIP6) experiment data, showing that it captures the temperature response in different locations with some limited accuracy in polar regions. We apply this approach to show local temperature change when a global mean temperature reaches 2°C.

1 Introduction

Evaluating uncertainty in coupled earth-society systems is important for understanding the impact of decision-making on society, and for developing metrics such as the social cost of carbon (SCC) (Interagency Working Group on Social Cost of Greenhouse Gases, United States Government, 2021; Carleton et al., 2022). One aspect of such uncertainty analysis involves evaluating the impacts of emissions trajectories from large ensembles of social scenarios to quantify impacts on the climate system. Because of the computational cost of running full-scale earth-system models, researchers rarely use them to evaluate large numbers of different emission scenarios. Detailed information drawn from these models, however, is useful for understanding the local climate impacts of decisions.

Current methods to evaluate the temperature response of the earth system to anthropogenic emissions of CO_2 include running global climate models (GCMs), earth system models (ESMs), earth system models of intermediate complexity (EMICs) (Claussen et al., 2002), energy balance models (EBMs) or multi-box models that underlie many integrated assessment models (IAMs). There is a tradeoff between model complexity (and thus the detail of results) and computational cost for all of these approaches. GCMs and ESMs are too computationally expensive to run large ensembles of policy scenarios. EMICs can evaluate the spatial temperature response to CO_2 emissions, with smaller computational costs due to lower resolution and reduced complexity physics. EBMs are computationally inexpensive, but provide only global mean or zonally-integrated representations of temperature changes.

The transient climate response to cumulative emissions of carbon dioxide (TCRE) (Matthews et al., 2009; Steinacher & Joos, 2016; Herrington & Zickfeld, 2014; Canadell et al., 2021) can be used to calculate the temperature impact of CO_2 emissions. Pattern scaling using the regional transient climate response to cumulative emissions of carbon dioxide (RTCRE) (Leduc et al., 2016) can provide low-cost, spatially explicit estimates of the temperature response to emissions. Applications of the RTCRE typically assume that the pattern response of temperature is constant and insensitive to the emissions trajectory, which can fail under varying emissions sizes and under reductions in emissions (Krasting et al., 2014; Zickfeld et al., 2016; Tokarska et al., 2019). This linearity and the TCRE have had important societal consequences, leading to the establishment of carbon budgets for a target global mean temperature (Meinshausen et al., 2009; Rogelj et al., 2011; Matthews et al., 2018; Matthews & Caldeira, 2008; Drake & Henderson, 2022).

Response operators, or Green's Functions, provide an alternate approach to diagnosing both global mean and spatial feedbacks to a forcing in ways that can capture differing pattern responses over time. Green's Functions have been used to characterize the radiative feedback response to sea surface temperature (Dong et al., 2019), temperature response to CO_2 concentrations (Lucarini et al., 2017; Lembo et al., 2020), and atmospheric transit times (Orbe et al., 2016). When diagnosed from ESMs, Green's Functions can form the basis for emulators that maintain the resolution of the original model, while reducing the computational load to simulate scenarios (as seen in Geoffroy and Saint-Martin (2014)).

Here, we construct an emulator, the Earth System Green's Response emulator (ESGR), of the pattern response of temperature to CO_2 emissions, which maintains the resolution of the ESMs it is derived from while enabling near-instantaneous computation. We take advantage of the approximately linear relationship between CO_2 emissions and temperature by diagnosing Green's Functions for temperature response to CO_2 emissions, using the Carbon Dioxide Removal Model Intercomparison Project (CDRMIP) model output (Keller et al., 2018). ESGR is based on the multi-model mean spatial Green's Function, and is evaluated with CMIP6 experiments. We show that it reproduces the temperature response due to emissions of CO_2 in most locations within one standard deviation of the CMIP6 multi-model mean both when CO_2 emissions are increasing and after their cessation. ESGR captures the time-dependent spatial patterns of the temperature response under two scenarios that end with the same cumulative CO_2 emissions. We illustrate how ESGR can be used to efficiently calculate metrics such as local temperature changes when a global mean 2 °C is reached.

2 Methods

We use model output from CDRMIP to build ESGR from calculated temperature responses to CO_2 emissions. Here we present the model data that is used to diagnose the Green's Functions and for evaluation, and explain the derivation and evaluation of ESGR.

2.1 CMIP6 Models

The Earth System Grid Federation (ESGF) archive includes six models that ran 250 years of pre-industrial control simulations (*esm-pi-ctrl*), as well as 100 gigaton carbon (GtC) pulse (*esm-pi-CO2pulse*) and removal (*esm-pi-CDRpulse*) emission simulations that branch from the *esm-pi-ctrl* at year 100 and allow the coupled carbon-climate system to respond over 90-140 years (Keller et al., 2018). There are six models with data from these experiments (shown in Table S1), each with two pulse scenarios (CanESM5 has 3 realizations of the pulse) for a total of 16 model runs. We compare ESGR to the difference between the *1pctCO*$_2$ or *esm-1pct-brch-1000PgC* experiment and the *esm-pi-ctrl* simulation for the same model source IDs as used to diagnose the Green's Function for evaluation (excluding GFDL as the data is unavaialable; see Table S2 for model information).

2.2 Spatial Green's Functions

We diagnose Green's Functions to create a spatiotemporally resolved pattern of temperature response to a CO_2 emissions pulse. In the case of CMIP6 experiment output, the change in the response variable of interest, T (near-surface air temperature at a location x), over time, is defined as:

$$\frac{\partial T(\mathbf{x})}{\partial t} = \mathcal{A}(T(\mathbf{x})) + E(t), \tag{1}$$

where $E(t)$ is the emissions forcing, and $\mathcal{A}(T)$ are the temperature tendency terms (everything impacting temperature aside from emissions, such as advection and radiation). Assuming that $\mathcal{A}(T)$ is independent of time and linear, we define a linear operator, $\mathcal{L} \equiv \frac{\partial}{\partial t} - \mathcal{A}$, that satisfies:

$$\mathcal{L}T(\mathbf{x}) = E(t). \tag{2}$$

A Green's Function, $G(\mathbf{x}, t-t')$, is defined as the response at location $\mathbf{x}$ and time t to an impulse (delta function) forcing at time $t = t'$ that satisfies the linear equation:

$$\mathcal{L}G(\mathbf{x}, t-t') = \delta(t-t'), \tag{3}$$

If we scale this by $E(t')$, and then integrate this over time, the resulting equation becomes:

$$\int \mathcal{L}G(\mathbf{x}, t-t')E(t')dt' = \int E(t')\delta(t-t')dt'. \tag{4}$$

Taking advantage of the assumed time-independence of $\mathcal{L}$, and that $\delta(t-t')$ is zero everywhere except where $t = t'$, we can simplify this as:

$$\mathcal{L}\left[\int G(\mathbf{x}, t-t')E(t')dt'\right] = E(t). \tag{5}$$

This takes the same form as 2, allowing us to equate

$$T(\mathbf{x}, t) = \int G(\mathbf{x}, t-t')E(t')dt', \tag{6}$$

providing a simple equation by which we can estimate the near-surface air temperature response given an emissions time series.

2.3 Diagnosing the Green's Functions from CMIP6

We can take this general form of the Green's Function and apply it to the CMIP6 pulse experiments. Here, $T_p(\mathbf{x}, t; t_0)$ is the temperature change due to either the *esm-pi-CO2pulse* or *esm-pi-CDRpulse* experiments relative to the *pi-ctrl*, and E_0 is the magnitude of the forcing from that pulse (100 or -100 GtC, respectively) at time t_0, resulting in:

$$\mathcal{L}T_p = E_0\delta(t-t_0). \tag{7}$$

Dividing equation 7 by the constant E_0, and using equation 3 we diagnose the Green's Function

$$G(\mathbf{x}, t - t_0) = \frac{T_p(\mathbf{x}, t; t_0)}{E_0}. \tag{8}$$

Assuming that G does not depend on the absolute time of the pulse, we can relabel the specific time t_0 to any time t', allowing us to convolve the Green's Function that is diagnosed in equation 8 with a forcing $E(t')$ at any time, as long as the scenario remains within present CO_2 states with up to 5000 GtC of cumulative emissions (as the linear relationship has been determined to hold to this level (Tokarska et al., 2016)).

Practically, we construct ESGR as the multi-model mean Green's Function for every grid box of the CMIP6 model output, equally weighting by model source ID. We use a 4th-order polynomial fit of the Green's Function to reduce the role of unforced internal variability (see Supplementary Information for an evaluation of unforced internal variability). In order to evaluate temperature response to a given emissions scenario, we convolve ESGR with emissions scenarios of CO_2 by summing the discretized integrands of equation 6 (using scipy's signal convolution (Virtanen et al., 2020)).

2.4 Evaluation

We evaluate ESGR with the *1pctCO$_2$* and *esm-1pct-brch-1000PgC* experiments. The *1pctCO$_2$* experiment prescribes a one percent increase in CO_2 concentration from pre-industrial conditions until four times the pre-industrial atmospheric concentration is reached (Eyring et al., 2016). The *esm-1pct-brch-1000PgC* experiment follows the *1pctCO$_2$* experiment until 1000PgC has accumulated in the atmosphere after which it allows the carbon cycle to freely evolve with zero anthropogenic CO_2 emissions.

We calculate the underlying emissions profiles for these two experiments according to methods described in equation 2 of (Liddicoat et al., 2021), where the emissions have to balance the atmospheric CO_2 concentration (G_{ATM}), exchange with the ocean (S_{OCEAN}), and exchange with the land ($S_{LAND} - E_{LUC}$):

$$E_{CO_2} = G_{ATM} + S_{OCEAN} + (S_{LAND} - E_{LUC}) \tag{9}$$

Where (G_{ATM}) is the co2mass variable, exchange with the ocean (S_{ocean}) is fgco2, and exchange with the land ($S_{land} - E_{LUC}$) is nbp, all globally integrated.

The evaluation is performed by 1) convolving individual model Green's Functions with the corresponding diagnosed *1pctCO$_2$* and *esm-1pct-brch-1000PgC* emissions profile, and 2) taking the weighted multi-model mean temperature response (weights are shown in Table S2). We convolve ESGR for each model ID and instance with the corresponding emissions and take the mean. ESGR depends in part on carbon cycle dynamics, so it has a non-zero correlation with the emissions that underlie an individual model's fixed CO_2 concentration experiments, and as a result, taking the mean before and after the convolution yield differing results. This is only necessary in the evaluation as emissions scenarios we independently create are not correlated to an individual model's response and can be convolved with the ESGR multi-model mean. We compare the ESGR near-surface air temperature response at every grid box with the weighted multi-model mean temperature difference between the *1pctCO$_2$* or the *esm-1pct-brch-1000PgC* experiment and the *pi-ctrl* run.

2.5 Smoothing approach for the Green's Function

We reduce the role of unforced internal variability by taking the mean across multiple models (Lehner & Deser, 2023), and by using a 4th-order polynomial fit (Lehner & Deser, 2023; Hawkins & Sutton, 2009) to the Green's Function (see Supplementary

Information and Figure S6 for a comparison of different fits to the Green's Function). The convolution also smooths out much of the high-frequency variability that is introduced in the Green's function approach (see Supplementary Information and Figure S8 for a discussion of the Fourier transform of the Green's function, which shows the reduction of this noise).

2.6 Transient Climate Response, Zero Emissions Commitment, and Pattern Scaling Calculations

We calculate a TCR for each model source ID using the temperature response of a *1pctCO*$_2$ experiment at a doubling of CO_2, defined as the mean between years 60 and 80 following the method of Matthews et al. (2009). The TCRE is the TCR divided by the cumulative emissions to year 70 in a *1pctCO*$_2$ experiment (Matthews et al., 2009). We use an approach similar to that of (MacDougall et al., 2020) for the ZEC, taking the twenty-year global mean temperature anomaly centered 15 years after cessation of emissions.

In order to pattern scale the TCRE, we multiply it by the cumulative emissions at every time (based on Leduc et al. (2016)'s RTCRE pattern scaling).

3 Results

We first present an evaluation of ESGR with respect to global mean and pattern response, comparing the temperature change to that of the multi-model mean CMIP6 for *1pctCO*$_2$ and *esm-1pctCO*$_2$*-brch-1000PgC* experiments. We then illustrate two potential applications, demonstrating how ESGR can be used for calculating the impact of varying emissions trajectories on warming, and show that we capture the dependence of the final state of surface temperature change on not only the cumulative emissions but also the time-dependent emissions pathway. Importantly, this emulator takes under one second to simulate 90 years of temperature response, which allows for the evaluation of a multitude of emissions trajectories.

3.1 Evaluation: Global Mean Response

Figure 1a shows that the global mean time series of ESGR is positive, and has a time mean value of 1.49°C/1000GtC, reflecting the expected warming response to emissions of CO_2. All of the individual model Green's Functions have a positive time-mean value over time, which is again expected given the positive temperature response to increased CO_2 emissions. ESGR reproduces the global mean temperature response over time to the *1pctCO*$_2$ and the *esm-1pctCO*$_2$*-brch-1000PgC* experiments (Figure 1b). It captures both the positive increase in temperature as a response to increasing CO_2 emissions, and the cessation of warming when emissions are stopped under *esm-1pctCO*$_2$*-brch-1000PgC*.

We quantify ESGR's ability to reproduce the global mean temperature change through calculating the TCR and ZEC for both the ESGR and CMIP6 experiments (Figure 1c and d). The multi-model mean TCR, which indicates the global mean warming after a doubling of CO_2, is 2.12°C for the CMIP6 *1pctCO*$_2$ experiments, and ESGR has a TCR of 2.04°C. The inter-model spread of ESGR, particularly the minimum and maximum, cover a larger range than in the CMIP6 experiments, due to the variability in ESGR's ability to capture global mean temperature response for individual models. The global mean ZEC for ESGR is -0.028, indicating a slight decrease in temperature after a cessation of emissions. This mean response falls within the inter-quartile range (IQR) of the CMIP6 experiments' ZEC; however, the mean CMIP6 ZEC indicates continued warming with a ZEC of 0.088.

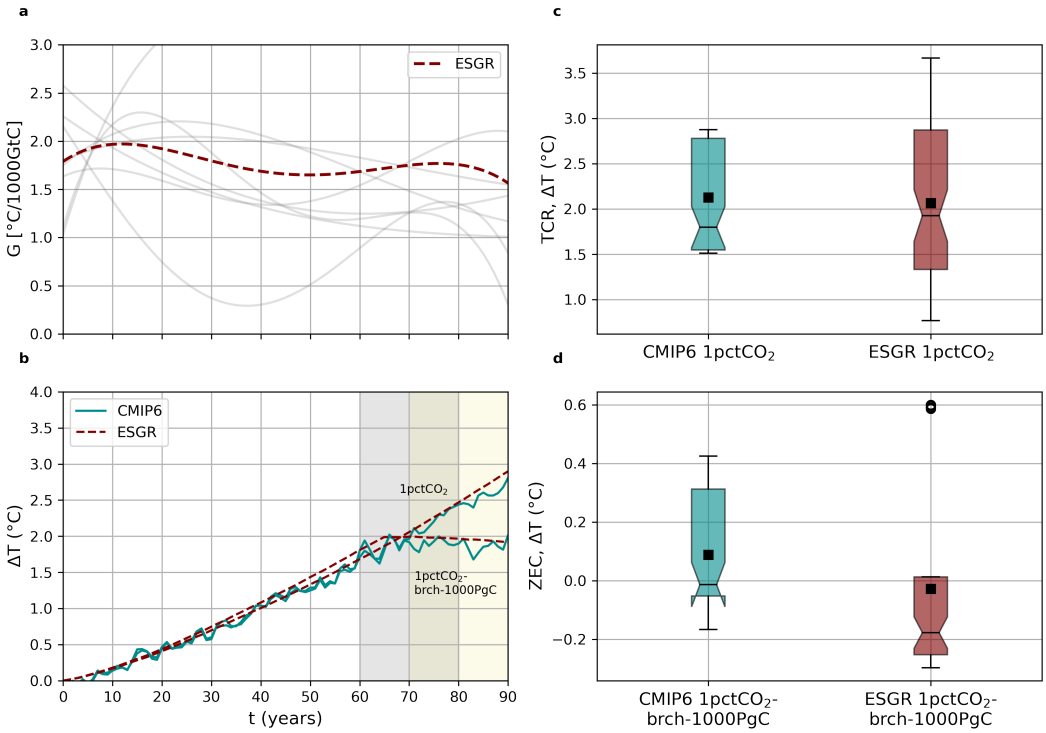

Figure 1. a) Global mean ESGR, and the spread of individual model Green's Functions. b) Mean of the *1pctCO*$_2$ and *esm-1pctCO*$_2$*-brch-1000PgC* emissions convolved with ESGR as compared to the multi-model mean of the *1pctCO*$_2$ and and *esm-1pctCO*$_2$*-brch-1000PgC* model runs compared to the *pi-ctrl*. Grey shading indicates the 20-year averaging period to calculate the TCR, and yellow shading indicates the 20-year time averaging period to calculate the ZEC. c and d) Mean, median, and interquartile range (IQR) of the TCR and ZEC (respectively).

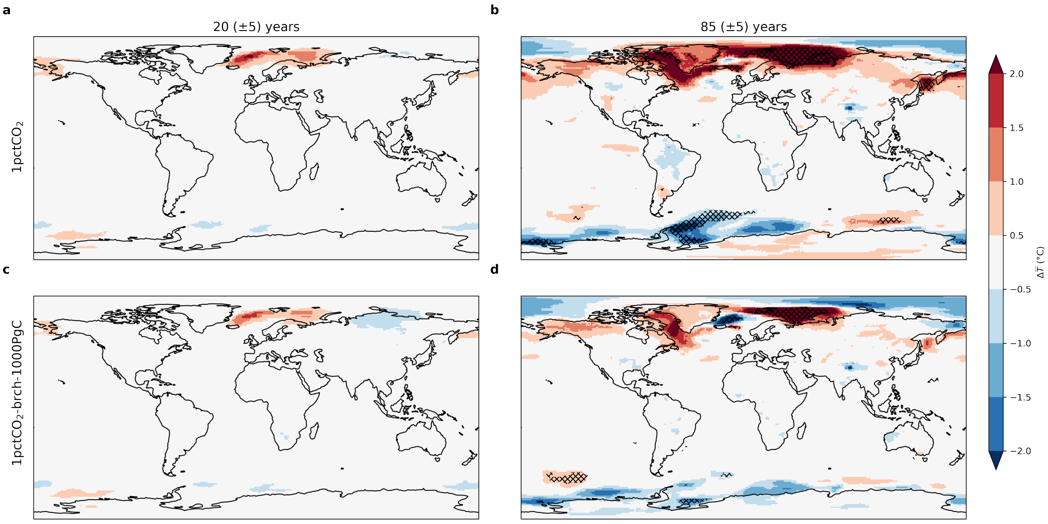

Figure 2. Difference in temperature response between ESGR *1pctCO$_2$* (top) or ESGR *esm-1pct-brch-1000PgC* (bottom) and the multi-model mean CMIP6 *1pctCO$_2$* or *esm-1pct-brch-1000PgC* experiment at 20(±5) and 85(±5) years. Hatching indicates locations that fall outside of a 1σ range of the model variability for the CMIP6 1pct model runs.

3.2 Evaluation: Pattern Response

Figure 2 shows the difference between the pattern response of ESGR and the multi-model mean CMIP6 *1pctCO$_2$* and *esm-1pctCO$_2$-brch-1000PgC* experiments at 20 (±5) and 85 (±5) years. ESGR is able to capture the temperature response to both *1pctCO$_2$* and *esm-1pctCO$_2$-brch-1000PgC* emissions over the first decade within 0.5°C of the CMIP6 model everywhere but the North Atlantic. After 20 years ESGR falls within one standard deviation of the CMIP6 model spread (Figure S5 shows the one standard deviation range), which we interpret as indicating the emulator is projecting a response consistent with the CMIP6 models. Over longer time periods, such as 85 years, ESGR is still able to capture the temperature response within 0.5°C of the CMIP6 experiments in all areas except for the Arctic and Antarctic due to nonlinearities from climate feedbacks (explored more in the Discussion and Conclusion). Even in the Arctic and Antarctic, many of the regions still fall within one standard deviation of the multi-model spread of CMIP6 responses; regions that are hatched are those that fall outside of this range. The temperature response in regions within one standard deviation of the multi-model mean CMIP6 responses are within the range of temperature responses that we would expect from an individual ESM. ESGR captures the reduced warming in year 85 of *esm-1pctCO$_2$-brch-1000PgC* as compared to the *1pctCO$_2$*, indicating that it can represent temperature response to both an increase and decrease in emissions (see Figure S4).

3.3 Application: Path-dependent Emissions Trajectories

ESGR can be used to show how emissions trajectories differ in their spatial temperature impact over time; here we calculate the outcomes of two example emissions scenarios that result in the same cumulative emissions. Trajectory 1 represents an increase in CO_2 emissions to 70 GtC/year over 20 years, followed by a rapid decline to zero GtC/year over 7 years, and Trajectory 2 represents an increase in CO_2 emissions to 37 GtC/year over 20 years, followed by a slow decline to zero GtC/year over 30 years. Both trajectories have the same cumulative emissions of 1050 GtC over a 120-year time span (Figure 3a). We convolve ESGR with these two trajectories creating *ESGR Traj 1* and *ESGR*

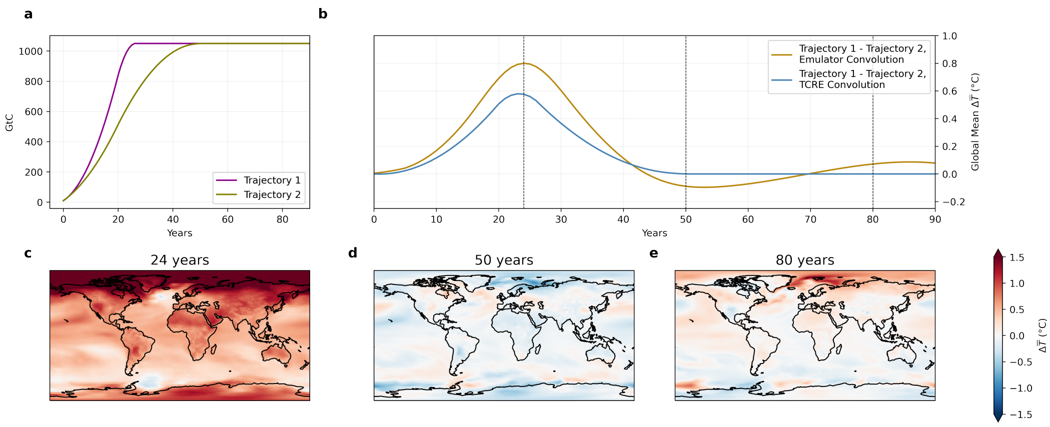

Figure 3. a) Cumulative emissions of CO_2 in GtC for 120 years in Trajectories 1 and 2. b) Global mean difference in temperature response to trajectories 1 and 2 convolved with either our Green's Function emulator or the TCRE. Dashed lines indicate years 24, 50, and 80 which are used in part c. c) The spatial pattern of the 10-year mean temperature difference between trajectories 1 and 2 convolved with our Green's Function emulator at years 24, 50, and 80 (all ± 5 years). The spatial pattern of temperature response by scaling the TCRE would have the same pattern of response throughout.

Traj 2. Figure 3 shows that at year 24, when the difference in cumulative emissions between the two scenarios is the greatest, there is more warming (both spatially and in the global mean) in *ESGR Traj 1* than *ESGR Traj 2*.

The calculated temperature response using ESGR is different than what results from scaling the TCRE by the cumulative emissions over time (as calculated in the Methods). This is expected, as the TCRE does not capture temperature responses when zero emissions are reached (Rogelj et al., 2018). Figure 3b shows that the peak temperature difference between Trajectories 1 and 2 is larger in ESGR than in a TCRE scaling, but the global mean temperature response does have a similar shape, as they both have peak differences in year 24. Once the two trajectories reach constant cumulative emissions, their global mean temperature in the TCRE convolution are, by definition, identical. However, there are fluctuations in the difference between *ESGR Traj 1* and *ESGR Traj 2* both in the global mean and spatially, capturing the emissions path dependency of warming (Krasting et al., 2014).

3.4 Application: Reaching Two Degrees of Warming

ESGR allows us to rapidly calculate the range of temperature response at different locations when a global mean temperature target is met under various emissions trajectories. We use the *1pctCO$_2$* and 6 additional trajectories (see Supplementary Information) that ramp up emissions more slowly but that reach the same cumulative emissions as 1pctCO2 has when the global mean temperature response is 2°C to show the local temperature dependence on historical emissions pathways. In ESGR *1pctCO$_2$*, when a 2°C global mean is reached after 69 years, Boston, Shanghai, Buenos Aires, and Lagos are at decadal mean temperatures of 2.68°C, 2.35°C, 1.66°C, and 1.77°C, respectively. Under scenarios that reach the same cumulative emissions by year 69, however, the decadal mean local temperatures could range between 1.49°-2.68 °C (Boston), 1.46°-2.35 °C (Shanghai), 0.90°-1.66 °C (Buenos Aires), and 1.03°-1.77 °C (Lagos). The variation in final temperature shows the dependency of local temperature on the trajectory of emissions. These

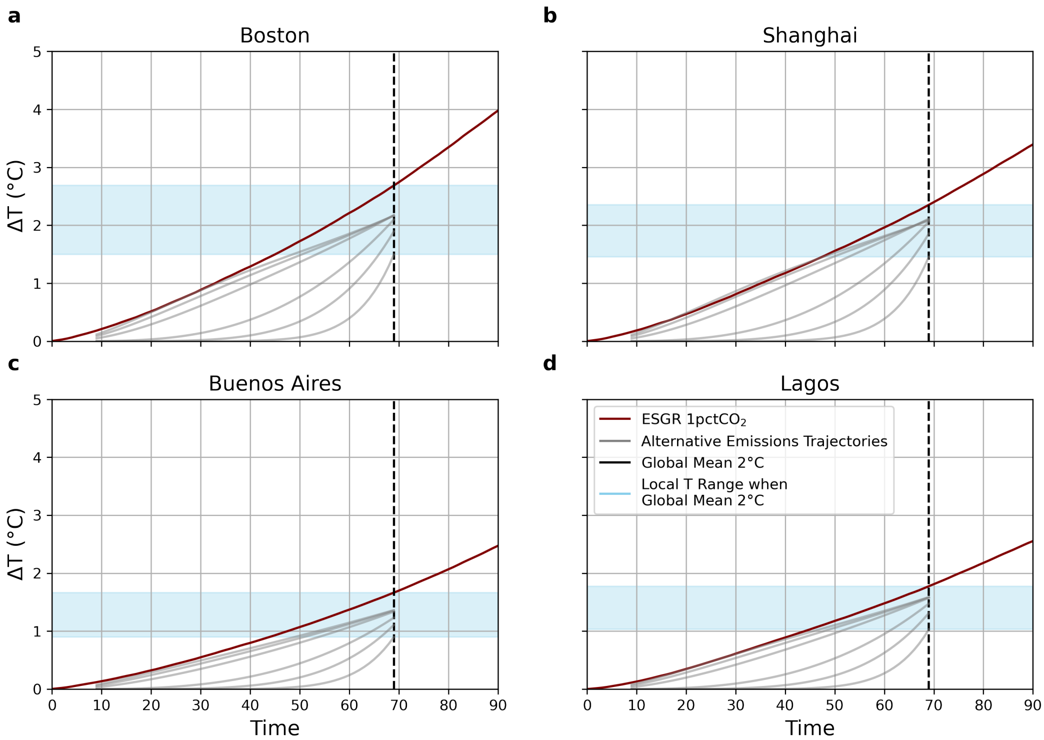

Figure 4. The time at which Boston, Shanghai, Buenos Aires, and Lagos reach 2 °C of warming. Black dashed lines show when the global mean temperature reaches 2°C. Horizontal blue shading indicates the local temperature range across our scenarios when a global mean of 2°C is reached. The emulated *1pctCO*$_2$ response is in maroon and light grey lines show the alternative scenarios that reach the same cumulative emissions (all shown as a ten year mean).

results would be strongly sensitive to the use of a scaling approach (such as pattern scaling the RTCRE), as a pattern scaling would yield the exact same temperature response in each location under the different emissions trajectories.

4 Discussion and Conclusions

Understanding the relationship between global emissions and local impacts is necessary for evaluating emissions trajectories under uncertainty, mitigating climate change, and adapting to a warming world. Here, we establish a Green's Function emulator (ESGR) for spatially resolved temperature responses to cumulative global CO_2 emissions. ESGR allows users to rapidly assess the local responses to policy options and their resulting global CO_2 emissions trajectories. We evaluate this approach, which builds on the linear relationships between cumulative emissions and temperature change, by identifying where it falls within the model spread of ESM's. We apply ESGR to two emissions trajectories and use it to examine the local temperature response when the global mean reaches 2°C under multiple scenarios.

ESGR captures the global and local temperature response to both increases and reductions in CO_2 emissions, suggesting that it reproduces the different timescales of the radiative and carbon cycle responses. It does worst at estimating temperature response at high latitudes, overestimating temperature changes in the Arctic, and underestimating temperature changes in the Southern Ocean. Arctic amplification is the higher rate of warming that is experienced in the Arctic (Pierrehumbert, 2010; Manabe & Wetherald, 1975; Budyko, 1969; Previdi et al., 2021; Henry et al., 2021). Our overestimate in the Arctic (Figure S3), indicates that in the process of linearizing the response of the climate system, we overestimate the positive feedbacks that would occur due to emissions of an additional unit of CO_2, or that unforced internal variability is captured in this approach. The Southern Ocean is understood to have delayed warming due to the overturning circulation and the transport of warm waters northward (Armour et al., 2016). We either overestimate the negative feedbacks that would occur due to the emissions of an additional unit of CO_2, or incorporate unforced internal variability that leads to this delayed warming, leading to an incorporation of too much Southern Ocean delayed warming. Although ESGR could include unforced internal variability due to a mismatch in variability between the *pi-ctrl* and *esm-pi-CO2pulse*/*esm-pi-CDRpulse* experiments, we take multiple approaches to reduce the impact of this noise (see Supplementary Information).

ESGR can be applied to rapidly calculate metrics that can explore the implications of path dependence of local temperature response to CO_2. Previous work has shown the importance of emission pathways due to nonlinearities in the climate system, particularly when CO_2 emissions are reduced after overshoot scenarios (e.g. Zickfeld et al. (2016); Tokarska et al. (2019)). Here, we are able to reproduce the path dependence of the linear response of temperature to cumulative emissions (Krasting et al., 2014). One potential underlying reason for this is the balance between the different spatial patterns of the fast and slow components of global warming, where a reduction in CO_2 forcing leads to a fast exponential response on the order of magnitude of a few years, as well as a slow, recalcitrant response that leads to up to 50% of CO_2 being removed from the atmosphere within 30 years, equilibration with the ocean occurring on century timescales, and weathering occurring on millennial timescales (Held et al., 2010; Joos et al., 2013; Denman et al., 2007; Glotter et al., 2014). ESGR is able to reproduce these fast and slow responses; the pulse of CO_2 it is based on causes both immediate changes in atmospheric CO_2 concentration while still allowing for slow ocean carbon and heat uptake (Figure S3 shows variations in ESGR over time).

Many of the limitations of ESGR are due to experiments and data available from the CMIP6 archive, and based on this work we can evaluate what would be necessary to build on this approach. ESGR is built on Green's Functions derived from pulse emissions from a pre-industrial background state, and prior work has shown that atmospheric CO_2 concentration response is dependent on the background CO_2 concentration (Joos et al., 2013). This dependency is offset by the logarithmic relationship between CO_2 concentration and radiative forcing, leading to the linear response of temperature to CO_2 emissions (Caldeira & Kasting, 1993). Furthermore, work has shown that this linear relationship between CO_2 cumulative emissions and temperature holds at up to 5000 GtC of cumulative emissions in ESMs (Tokarska et al., 2016). Pulses of various sizes have been shown to influence the rate of the temperature response (Steinacher & Joos, 2016). However, the impact of emissions size is smaller than the impact of using various models (Krasting et al., 2014). As a result, the linear response function we derive here should be robust across varying background concentrations of CO_2 and emission sizes.

These assumptions could be better tested with additional ESM experiments to quantify the impact of pulse size, background state, short and long responses of the climate system, and internal variability. Additional ESM experiments pulsing varying sizes of emissions from a different starting condition would allow for quantification of the impact of the pulse size and background state– currently, the closest available experiments are the *CDR-yr2010-pulse* experiments, which are not publicly available on the Earth System Grid Federation (ESGF) and have been run in EMICs. If the pulse (*esm-pi-CO2pulse*) and removal (*esm-pi-CDRpulse*) experiments were run for longer time periods, this would improve our ability to evaluate long timescales and estimate variations in the ZEC over time (MacDougall et al., 2020). Lastly, an ensemble of pulse emissions from individual models would allow for better quantification of the role of internal variability, and for averaging out its impact on the Green's Function. As climate models improve, and as more become available, ESGR can be updated easily to reflect the latest state of the science.

Open Research Section

All code to reproduce this work is available on Zenodo (currently available on github at `https://github.com/lfreese/CO2_greens`, to be updated to Zenodo for publication). The raw data from CMIP6 is available at `https://esgf-node.llnl.gov/search/cmip6/`, and all of the experiments and runs used are described in Tables S1 and S2.

Acknowledgments

Author Contributions: Conceptualization: LF; Method development: LF; Analysis: LF; Interpretation: LF, NS, AF; Writing-original draft: LF; Writing-edits and review: LF, NS, AF; Supervision: NS.

We thank the NIEHS Toxicology Training Grant no. T32-ES007020 and the MIT Martin Family Society of Fellows for Sustainability (L.M.F.). This work was supported in part by the MIT Climate Grand Challenges project "Bringing Computation to the Climate Challenge" (L.M.F., N.E.S., and A.M.F.).

References

Armour, K. C., Marshall, J., Scott, J. R., Donohoe, A., & Newsom, E. R. (2016, July). Southern Ocean warming delayed by circumpolar upwelling and equatorward transport. *Nature Geoscience*, *9*(7), 549–554. Retrieved 2023-03-28, from `https://www.nature.com/articles/ngeo2731` (Number: 7 Publisher: Nature Publishing Group) doi: 10.1038/ngeo2731

Budyko, M. I. (1969, January). The effect of solar radiation variations on the climate of the Earth. , *21*(5), 611. Retrieved 2023-04-18, from `https://a.tellusjournals.se/articles/10.3402/tellusa.v21i5.10109` (Number: 5 Publisher: Stockholm University Press) doi: 10.3402/tellusa.v21i5.10109

Caldeira, K., & Kasting, J. F. (1993, November). Insensitivity of global warming potentials to carbon dioxide emission scenarios. *Nature*, *366*(6452), 251–253. Retrieved 2023-04-18, from `https://www.nature.com/articles/366251a0` (Number: 6452 Publisher: Nature Publishing Group) doi: 10.1038/366251a0

Canadell, J., Monteiro, P., Costa, M., da Cunha, L. C., Cox, P., Eliseev, A., ... Zickfeld, a. K. (2021). Global Carbon and other Biogeochemical Cycles and Feedbacks. *Climate Change 2021: The Physical Science Basis. Contribution of Working Group I to the Sixth Assessment Report of the Intergovernmental Panel on Climate Change*, 673–816. ([Masson-Delmotte, V., P. Zhai, A. Pirani, S.L. Connors, C. Péan, S. Berger, N. Caud, Y. Chen, L. Goldfarb, M.I. Gomis, M. Huang, K. Leitzell, E. Lonnoy, J.B.R. Matthews, T.K. Maycock, T. Waterfield, O. Yelekçi, R. Yu, and B. Zhou (eds.)]) doi: 10.1017/9781009157896.007

Carleton, T., Jina, A., Delgado, M., Greenstone, M., Houser, T., Hsiang, S., ... Zhang, A. T. (2022, November). Valuing the Global Mortality Consequences of Climate Change Accounting for Adaptation Costs and Benefits. *The Quarterly Journal of Economics*, *137*(4), 2037–2105. Retrieved 2022-12-09, from `https://doi.org/10.1093/qje/qjac020` doi: 10.1093/qje/qjac020

Claussen, M., Mysak, L., Weaver, A., Crucifix, M., Fichefet, T., Loutre, M.-F., ... Wang, Z. (2002, March). Earth system models of intermediate complexity: closing the gap in the spectrum of climate system models. *Climate Dynam-*

ics, *18*(7), 579–586. Retrieved 2023-03-29, from https://doi.org/10.1007/s00382-001-0200-1 doi: 10.1007/s00382-001-0200-1

Denman, K. L., Brasseur, G., Chidthaisong, A., Ciais, P., Cox, P. M., Dickinson, R. E., ... Molina, M. (2007). *Couplings Between Changes in the Climate System and Biogeochemistry* (Climate Change 2007: The Physical Science Basis). Cambridge University Press, Cambridge, United Kingdom and New York, NY, USA..

Dong, Y., Proistosescu, C., Armour, K., & Battisti, D. (2019). Attributing Historical and Future Evolution of Radiative Feedbacks to Regional Warming Patterns using a Green's Function Approach: The Preeminence of the Western Pacific. *Journal of Climate*, *Volume 32*(Issue 17). Retrieved 2022-07-08, from https://journals.ametsoc.org/view/journals/clim/32/17/jcli-d-18-0843.1.xml

Drake, H. F., & Henderson, G. (2022, May). A defense of usable climate mitigation science: how science can contribute to social movements. *Climatic Change*, *172*(1), 10. Retrieved 2022-11-25, from https://doi.org/10.1007/s10584-022-03347-6 doi: 10.1007/s10584-022-03347-6

Eyring, V., Bony, S., Meehl, G. A., Senior, C. A., Stevens, B., Stouffer, R. J., & Taylor, K. E. (2016, May). Overview of the Coupled Model Intercomparison Project Phase 6 (CMIP6) experimental design and organization. *Geoscientific Model Development*, *9*(5), 1937–1958. Retrieved 2023-03-13, from https://gmd.copernicus.org/articles/9/1937/2016/ (Publisher: Copernicus GmbH) doi: 10.5194/gmd-9-1937-2016

Geoffroy, O., & Saint-Martin, D. (2014, December). Pattern decomposition of the transient climate response. *Tellus A: Dynamic Meteorology and Oceanography*, *66*(1), 23393. Retrieved 2023-04-18, from https://a.tellusjournals.se/article/10.3402/tellusa.v66.23393/ doi: 10.3402/tellusa.v66.23393

Glotter, M. J., Pierrehumbert, R. T., Elliott, J. W., Matteson, N. J., & Moyer, E. J. (2014, October). A simple carbon cycle representation for economic and policy analyses. *Climatic Change*, *126*(3), 319–335. Retrieved 2023-04-18, from https://doi.org/10.1007/s10584-014-1224-y doi: 10.1007/s10584-014-1224-y

Hawkins, E., & Sutton, R. (2009, August). The Potential to Narrow Uncertainty in Regional Climate Predictions. *Bulletin of the American Meteorological Society*, *90*(8), 1095–1108. Retrieved 2023-05-30, from https://journals.ametsoc.org/view/journals/bams/90/8/2009bams2607_1.xml (Publisher: American Meteorological Society Section: Bulletin of the American Meteorological Society) doi: 10.1175/2009BAMS2607.1

Held, I. M., Winton, M., Takahashi, K., Delworth, T., Zeng, F., & Vallis, G. K. (2010, May). Probing the Fast and Slow Components of Global Warming by Returning Abruptly to Preindustrial Forcing. *Journal of Climate*, *23*(9), 2418–2427. Retrieved 2023-02-13, from https://journals.ametsoc.org/view/journals/clim/23/9/2009jcli3466.1.xml (Publisher: American Meteorological Society Section: Journal of Climate) doi: 10.1175/2009JCLI3466.1

Henry, M., Merlis, T. M., Lutsko, N. J., & Rose, B. E. J. (2021, March). Decomposing the Drivers of Polar Amplification with a Single-Column Model. *Journal of Climate*, *34*(6), 2355–2365. Retrieved 2023-04-24, from https://journals.ametsoc.org/view/journals/clim/34/6/JCLI-D-20-0178.1.xml (Publisher: American Meteorological Society Section: Journal of Climate) doi: 10.1175/JCLI-D-20-0178.1

Herrington, T., & Zickfeld, K. (2014, November). Path independence of climate and carbon cycle response over a broad range of cumulative carbon emissions. *Earth System Dynamics*, *5*(2), 409–422. Retrieved 2023-02-14, from https://esd.copernicus.org/articles/5/409/2014/ (Publisher: Copernicus GmbH) doi: 10.5194/esd-5-409-2014

Interagency Working Group on Social Cost of Greenhouse Gases, United States Government. (2021). *Technical Support Document: Social Cost of Carbon, Methane, and Nitrous Oxide.* Retrieved 2022-12-13, from https://web.archive.org/web/20221212061639/https://www.whitehouse.gov/wp-content/uploads/2021/02/TechnicalSupportDocument_SocialCostofCarbonMethaneNitrousOxide.pdf

Joos, F., Roth, R., Fuglestvedt, J. S., Peters, G. P., Enting, I. G., von Bloh, W., ... Weaver, A. J. (2013, March). Carbon dioxide and climate impulse response functions for the computation of greenhouse gas metrics: a multi-model analysis. *Atmospheric Chemistry and Physics*, *13*(5), 2793–2825. Retrieved 2020-12-16, from https://acp.copernicus.org/articles/13/2793/2013/ doi: 10.5194/acp-13-2793-2013

Keller, D. P., Lenton, A., Scott, V., Vaughan, N. E., Bauer, N., Ji, D., ... Zickfeld, K. (2018, March). The Carbon Dioxide Removal Model Intercomparison Project (CDRMIP): rationale and experimental protocol for CMIP6. *Geoscientific Model Development*, *11*(3), 1133–1160. Retrieved 2022-11-04, from https://gmd.copernicus.org/articles/11/1133/2018/ (Publisher: Copernicus GmbH) doi: 10.5194/gmd-11-1133-2018

Krasting, J. P., Dunne, J. P., Shevliakova, E., & Stouffer, R. J. (2014). Trajectory sensitivity of the transient climate response to cumulative carbon emissions. *Geophysical Research Letters*, *41*(7), 2520–2527. Retrieved 2023-03-29, from https://onlinelibrary.wiley.com/doi/abs/10.1002/2013GL059141 (_eprint: https://agupubs.onlinelibrary.wiley.com/doi/pdf/10.1002/2013GL059141) doi: 10.1002/2013GL059141

Leduc, M., Matthews, H. D., & de Elía, R. (2016, May). Regional estimates of the transient climate response to cumulative CO2 emissions. *Nature Climate Change*, *6*(5), 474–478. Retrieved 2023-01-30, from https://www.nature.com/articles/nclimate2913 (Number: 5 Publisher: Nature Publishing Group) doi: 10.1038/nclimate2913

Lehner, F., & Deser, C. (2023, May). Origin, importance, and predictive limits of internal climate variability. *Environmental Research: Climate*, *2*(2), 023001. Retrieved 2023-05-24, from https://dx.doi.org/10.1088/2752-5295/accf30 (Publisher: IOP Publishing) doi: 10.1088/2752-5295/accf30

Lembo, V., Lucarini, V., & Ragone, F. (2020, December). Beyond Forcing Scenarios: Predicting Climate Change through Response Operators in a Coupled General Circulation Model. *Scientific Reports*, *10*(1), 8668. Retrieved 2021-03-31, from http://www.nature.com/articles/s41598-020-65297-2 doi: 10.1038/s41598-020-65297-2

Liddicoat, S. K., Wiltshire, A. J., Jones, C. D., Arora, V. K., Brovkin, V., Cadule, P., ... Ziehn, T. (2021, April). Compatible Fossil Fuel CO2 Emissions in the CMIP6 Earth System Models' Historical and Shared Socioeconomic Pathway Experiments of the Twenty-First Century. *Journal of Climate*, *34*(8), 2853–2875. Retrieved 2022-11-04, from https://journals.ametsoc.org/view/journals/clim/34/8/JCLI-D-19-0991.1.xml (Publisher: American Meteorological Society Section: Journal of Climate) doi: 10.1175/JCLI-D-19-0991.1

Lucarini, V., Ragone, F., & Lunkeit, F. (2017, February). Predicting Climate Change Using Response Theory: Global Averages and Spatial Patterns. *Journal of Statistical Physics*, *166*(3-4), 1036–1064. Retrieved 2021-03-31, from http://link.springer.com/10.1007/s10955-016-1506-z doi: 10.1007/s10955-016-1506-z

MacDougall, A. H., Frölicher, T. L., Jones, C. D., Rogelj, J., Matthews, H. D., Zickfeld, K., ... Ziehn, T. (2020, June). Is there warming in the pipeline? A multi-model analysis of the Zero Emissions Commitment from CO_2. *Biogeosciences*, *17*(11), 2987–3016. Retrieved 2023-03-15, from https://

bg.copernicus.org/articles/17/2987/2020/ (Publisher: Copernicus GmbH) doi: 10.5194/bg-17-2987-2020

Manabe, S., & Wetherald, R. T. (1975, January). The Effects of Doubling the CO2 Concentration on the climate of a General Circulation Model. *Journal of the Atmospheric Sciences*, *32*(1), 3–15. Retrieved 2023-04-18, from https://journals.ametsoc.org/view/journals/atsc/32/1/1520-0469_1975_032_0003_teodtc_2_0_co_2.xml (Publisher: American Meteorological Society Section: Journal of the Atmospheric Sciences) doi: 10.1175/1520-0469(1975)032⟨0003:TEODTC⟩2.0.CO;2

Matthews, H. D., & Caldeira, K. (2008). Stabilizing climate requires near-zero emissions. *Geophysical Research Letters*, *35*(4). Retrieved 2022-11-04, from https://onlinelibrary.wiley.com/doi/abs/10.1029/2007GL032388 (_eprint: https://onlinelibrary.wiley.com/doi/pdf/10.1029/2007GL032388) doi: 10.1029/2007GL032388

Matthews, H. D., Gillett, N. P., Stott, P. A., & Zickfeld, K. (2009, June). The proportionality of global warming to cumulative carbon emissions. *Nature*, *459*(7248), 829–832. Retrieved 2022-11-04, from https://www.nature.com/articles/nature08047 (Number: 7248 Publisher: Nature Publishing Group) doi: 10.1038/nature08047

Matthews, H. D., Zickfeld, K., Knutti, R., & Allen, M. R. (2018, January). Focus on cumulative emissions, global carbon budgets and the implications for climate mitigation targets. *Environmental Research Letters*, *13*(1), 010201. Retrieved 2023-02-15, from https://dx.doi.org/10.1088/1748-9326/aa98c9 (Publisher: IOP Publishing) doi: 10.1088/1748-9326/aa98c9

Meinshausen, M., Meinshausen, N., Hare, W., Raper, S. C. B., Frieler, K., Knutti, R., . . . Allen, M. R. (2009, April). Greenhouse-gas emission targets for limiting global warming to 2 °C. *Nature*, *458*(7242), 1158–1162. Retrieved 2023-04-18, from https://www.nature.com/articles/nature08017 (Number: 7242 Publisher: Nature Publishing Group) doi: 10.1038/nature08017

Orbe, C., Waugh, D. W., Newman, P. A., & Steenrod, S. (2016, October). The Transit-Time Distribution from the Northern Hemisphere Midlatitude Surface. *Journal of the Atmospheric Sciences*, *73*(10), 3785–3802. Retrieved 2022-07-12, from https://journals.ametsoc.org/view/journals/atsc/73/10/jas-d-15-0289.1.xml (Publisher: American Meteorological Society Section: Journal of the Atmospheric Sciences) doi: 10.1175/JAS-D-15-0289.1

Pierrehumbert, R. (2010). 4.4: Real gas radiation: basic principles. In *Principles of Planetary Climate.* New York: Cambridge University Press.

Previdi, M., Smith, K. L., & Polvani, L. M. (2021, September). Arctic amplification of climate change: a review of underlying mechanisms. *Environmental Research Letters*, *16*(9), 093003. Retrieved 2023-04-24, from https://dx.doi.org/10.1088/1748-9326/ac1c29 (Publisher: IOP Publishing) doi: 10.1088/1748-9326/ac1c29

Rogelj, J., Hare, W., Lowe, J., van Vuuren, D. P., Riahi, K., Matthews, B., . . . Meinshausen, M. (2011, November). Emission pathways consistent with a 2 °C global temperature limit. *Nature Climate Change*, *1*(8), 413–418. Retrieved 2023-04-18, from https://www.nature.com/articles/nclimate1258 (Number: 8 Publisher: Nature Publishing Group) doi: 10.1038/nclimate1258

Rogelj, J., Shindell, D., Jiang, K., Fifita, S., Forster, P., Ginzburg, V., . . . Vilariño, M. (2018). *Mitigation Pathways Compatible with 1.5°C in the Context of Sustainable Development. In: Global Warming of 1.5°C. An IPCC Special Report on the impacts of global warming of 1.5°C above pre-industrial levels and related global greenhouse gas emission pathways, in the context of strengthening the global response to the threat of climate change, sustainable development, and efforts to eradicate poverty.*

Steinacher, M., & Joos, F. (2016, February). Transient Earth system responses to cumulative carbon dioxide emissions: linearities, uncertainties, and probabilities in an observation-constrained model ensemble. *Biogeosciences*, *13*(4), 1071–1103. Retrieved 2023-02-14, from `https://bg.copernicus.org/articles/13/1071/2016/bg-13-1071-2016-discussion.html` (Publisher: Copernicus GmbH) doi: 10.5194/bg-13-1071-2016

Tokarska, K. B., Gillett, N. P., Weaver, A. J., Arora, V. K., & Eby, M. (2016, September). The climate response to five trillion tonnes of carbon. *Nature Climate Change*, *6*(9), 851–855. Retrieved 2023-03-09, from `https://www.nature.com/articles/nclimate3036` (Number: 9 Publisher: Nature Publishing Group) doi: 10.1038/nclimate3036

Tokarska, K. B., Zickfeld, K., & Rogelj, J. (2019). Path Independence of Carbon Budgets When Meeting a Stringent Global Mean Temperature Target After an Overshoot. *Earth's Future*, *7*(12), 1283–1295. Retrieved 2023-03-24, from `https://onlinelibrary.wiley.com/doi/abs/10.1029/2019EF001312` (_eprint: https://onlinelibrary.wiley.com/doi/pdf/10.1029/2019EF001312) doi: 10.1029/2019EF001312

Virtanen, P., Gommers, R., Oliphant, T. E., Haberland, M., Reddy, T., Cournapeau, D., ... van Mulbregt, P. (2020, March). SciPy 1.0: fundamental algorithms for scientific computing in Python. *Nature Methods*, *17*(3), 261–272. Retrieved 2022-11-04, from `https://www.nature.com/articles/s41592-019-0686-2` (Number: 3 Publisher: Nature Publishing Group) doi: 10.1038/s41592-019-0686-2

Zickfeld, K., MacDougall, A. H., & Matthews, H. D. (2016, May). On the proportionality between global temperature change and cumulative CO2 emissions during periods of net negative CO2 emissions. *Environmental Research Letters*, *11*(5), 055006. Retrieved 2023-03-24, from `https://dx.doi.org/10.1088/1748-9326/11/5/055006` (Publisher: IOP Publishing) doi: 10.1088/1748-9326/11/5/055006

Supporting Information for “Spatially Resolved Temperature Response Functions to CO_2 Emissions”

Lyssa M. Freese [1], Arlene M. Fiore [1], Noelle E. Selin [1,2]

[1]Massachusetts Institute of Technology, Earth, Atmospheric, and Planetary Sciences

[2]Massachusetts Institute of Technology, Institute for Data, Systems, and Society

Contents of this file

1. Text S1 to S3
2. Figures S1 to S8
3. Tables S1 to S2

Introduction

Text S1: Green’s Function Analysis

Figure S1 shows that the individual model Green’s Functions are different if they are diagnosed from the *esm-pi-CO2pulse* versus the *esm-pi-CDRpulse* experiments. This difference could be due to a variety of reasons, including our limitation to only an individual model run (except in the case of CANESM), or non-linearities in the way CO_2 and heat are taken up versus released by the land and ocean. These individual model Green’s

Functions vary in their ability to reconstruct the temperature response to the *1pctCO*$_2$ experiment (see Figure S2).

We evaluate the difference between the first thirty and final sixty years of ESGR (scaled by the initial emissions size, 100 GtC) in Figure S3. We split the Green's Function into these two time periods based on (Joos et al., 2013)– defining an initial immediate response over the first four years, and a slower response over the following 32 years. We see increased warming in the poles in the later response time period, in contrast to enhanced warming over land areas in the immediate time period of 0-4 years, as has been explored in (Held et al., 2010).

Text S2: Green's Function Sensitivity to the Smoothing Approach

We use a 4th-order polynomial fit to our Green's Function to reduce the role of internal variability. Here we discuss the sensitivity of this fit as compared to other smoothing approaches, and the role of the convolution in smoothing out internal variability.

In order to minimize the impact of this difference in unforced internal variability that arises, we take a number of steps: 1) averaging across multiple models and realizations, 2) smoothing the Green's function with a 4th-order polynomial fit, 3) comparing ESGR to a Green's function diagnosed from a pulse run and just the climatology of the *pi-ctrl*, and 4) comparing internal variability within models to the inter-model spread. Additionally, the process of the convolution itself also reduces the impact of this internal variability, as positive and negative phases can cancel each other out.

We test the sensitivity of our smoothing approach by comparing the 4th-order polynomial fit to five different Green's Functions (a-e): a) a Green's Function diagnosed by using the 100 gigaton carbon (GtC) pulse (*esm-pi-CO2pulse*) and removal (*esm-pi-CDRpulse*) emission simulations and the *pi-ctrl* simulation; b, c, and d) a 5, 10, and 30-year rolling mean Green's Function, and e) Green's Function diagnosed by using the *esm-pi-CO2pulse* and *esm-pi-CDRpulse* emission simulations and the climatology of the *pi-ctrl* simulation. The comparison to the varying rolling means tests the sensitivity of the timescale of our smoothing approach. Using the climatology for the *pi-ctrl* is a potential way to reduce unforced internal variability in the resulting Green's Function, although it can also falsely attribute drift in the *pi-ctrl* as a signal. Figure S6 shows the impact of various timescales for taking the rolling mean and for a 4th-order polynomial fit of the Green's Function. Much of the noise is canceled out in both the 4th-order polynomial and the 30-year rolling mean, but the curve still maintains a similar magnitude and trend. We then test the impact of these differences on the results of a convolution; once convolved with emissions from a $1pctCO_2$ experiment, the spatial temperature change for each of these six Green's Functions are very similar. Figure S7 shows the root mean squared error (RMSE) for predicted temperatures versus the expected temperatures in a $1pctCO_2$ experiment using the temperature change from each of the six Green's Functions. The RMSE is calculated as: $\sqrt{\sum_{i=0}^{N} \frac{(predicted_i - expected_i)^2}{N}}$, where N is the number of years (limited to 90), the predicted values are temperatures from a convolution, and the expected values are temperatures from the multi-model mean CMIP6 $1pctCO_2$ experiment. The global mean RMSE is lowest for a 4th-order polynomial fit, but as seen in Figure S7, they are all within a similar range of values.

To test whether or not the convolution is reducing the noise, we can take the Fourier transform of our global mean ESGR and of the emissions from a multi-model mean *1pct-CO_2* experiment. Because of the convolution theorem, we know that the Fourier transform of the convolution of these functions is equal to the product of their Fourier transforms. Figure S8 shows the Fourier transform of ESGR, where it is clear that there is a strong low-frequency signal, as well as a number of weaker high-frequency signals that indicate either forced or unforced internal variability. The Fourier transform of the function of the emissions similarly has a strong low-frequency signal and very few weak high-frequency signals. The product of these two dampens these higher-frequency signals; since the product of the Fourier transforms is the same as the Fourier transform of their convolution, we can say that the high-frequency noise (internal variability), is being reasonably reduced by the convolution process.

Text S3: Trajectory Creation

We create six trajectories that have the same cumulative emissions as the *1pctCO_2* experiment by the year a global mean 2°C is reached (year 69). These trajectories are meant to exemplify the importance of historical emissions on temperature outcomes, and are idealized smooth power-law fits of emissions that follow the equation:

$$e(t) = \frac{(c(n+1)t^n)}{t_f^{n+1}} \tag{1}$$

scaled such that $\int_{t=0}^{t_f} e(t)dt = c$, where c is the cumulative emissions desired (1204.7 GtC), t is the time range of emissions (0-90 years), t_f is the time by which c is reached (69 years), and n is polynomial fit desired. We calculate the emissions for n = 1/8, 1/4, 1/2, 2, 4, and 8.

References

Held, I. M., Winton, M., Takahashi, K., Delworth, T., Zeng, F., & Vallis, G. K. (2010, May). Probing the Fast and Slow Components of Global Warming by Returning Abruptly to Preindustrial Forcing. *Journal of Climate*, *23*(9), 2418–2427. Retrieved 2023-02-13, from `https://journals.ametsoc.org/view/journals/clim/23/9/2009jcli3466.1.xml` (Publisher: American Meteorological Society Section: Journal of Climate) doi: 10.1175/2009JCLI3466.1

Joos, F., Roth, R., Fuglestvedt, J. S., Peters, G. P., Enting, I. G., von Bloh, W., ... Weaver, A. J. (2013, March). Carbon dioxide and climate impulse response functions for the computation of greenhouse gas metrics: a multi-model analysis. *Atmospheric Chemistry and Physics*, *13*(5), 2793–2825. Retrieved 2020-12-16, from `https://acp.copernicus.org/articles/13/2793/2013/` doi: 10.5194/acp-13-2793-2013

Table S1. Model Information for Green's Function Derivation. *Italicization indicates that the realizations that are in italics only have the Experiment IDs italicized.*

Model	Realizations	Experiment IDs	Data Variables	Frequency	Weighting Function
GFDL	r1i1f1p1	esm-pictrl, esm-pi-CO2pulse, esm-pi-cdr-pulse	tas	monthly	1
NORESM2	r1i1f1p1	esm-pictrl, esm-pi-CO2pulse, esm-pi-cdr-pulse	tas	monthly	1
UKESM1	r1i1f2p1	esm-pictrl, esm-pi-CO2pulse, esm-pi-cdr-pulse	tas	monthly	1
CanESM5	r1i1f1p2, *r2i1f1p2*, *r3i1f1p2*	esm-pictrl, *esm-pi-CO2pulse*, *esm-pi-cdr-pulse*	tas	monthly	1/3, 1/3, 1/3
ACCESS	r1i1f1p1	esm-pictrl, esm-pi-CO2pulse, esm-pi-cdr-pulse	tas	monthly	1
MIROC	r1i1f2p1	esm-pictrl, esm-pi-CO2pulse, esm-pi-cdr-pulse	tas	monthly	1

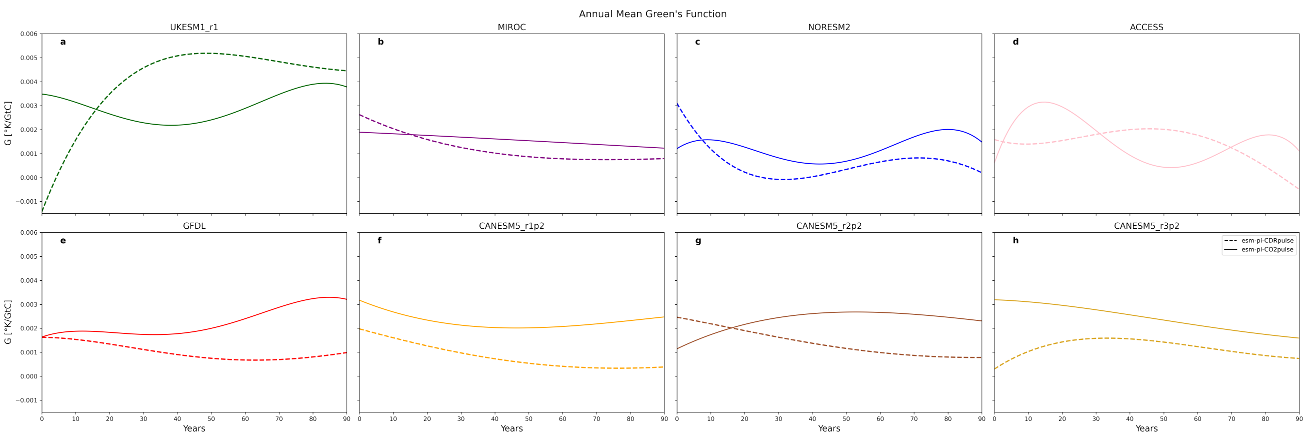

Figure S1. 4th-order polynomial fit global mean Green's Function for every model in both the *esm-pi-CO2pulse* and *esm-pi-CDRpulse*.

Table S2. Model Information for 1pctCO_2 Comparison

Model	Realizations	Experiment IDs	Data Variables	Frequency	Weighting Function
GFDL	r1i1f1p1	pictrl, 1pctCO2	tas, co2mass, fgco2, nbp, areacella	monthly	1
NORESM2	r1i1f1p1	pictrl, 1pctCO2, esm-1pct-brch-1000PgC	tas, co2mass, fgco2, nbp, areacello, areacella	monthly	1
UKESM1	r1i1f2p1, r2i1f2p1, r3i1f2p1, r4i1f2p1	pictrl, 1pctCO2, esm-1pct-brch-1000PgC	tas, co2mass, fgco2, nbp, areacello, areacella	monthly	1/4 1/4 1/4 1/4
CanESM5	r1i1f1p2, r2i1f1p2, r3i1f1p2	pictrl, 1pctCO2, esm-1pct-brch-1000PgC	tas, fgco2, nbp, areacello, areacella	monthly	1/3, 1/3, 1/3
ACCESS	r1i1f1p1	pictrl, 1pctCO2, esm-1pct-brch-1000PgC	tas, fgco2, nbp, areacello, areacella	monthly	1
MIROC	r1i1f2p1	pictrl, 1pctCO2, esm-1pct-brch-1000PgC	tas, fgco2, nbp, areacello, areacella	monthly	1

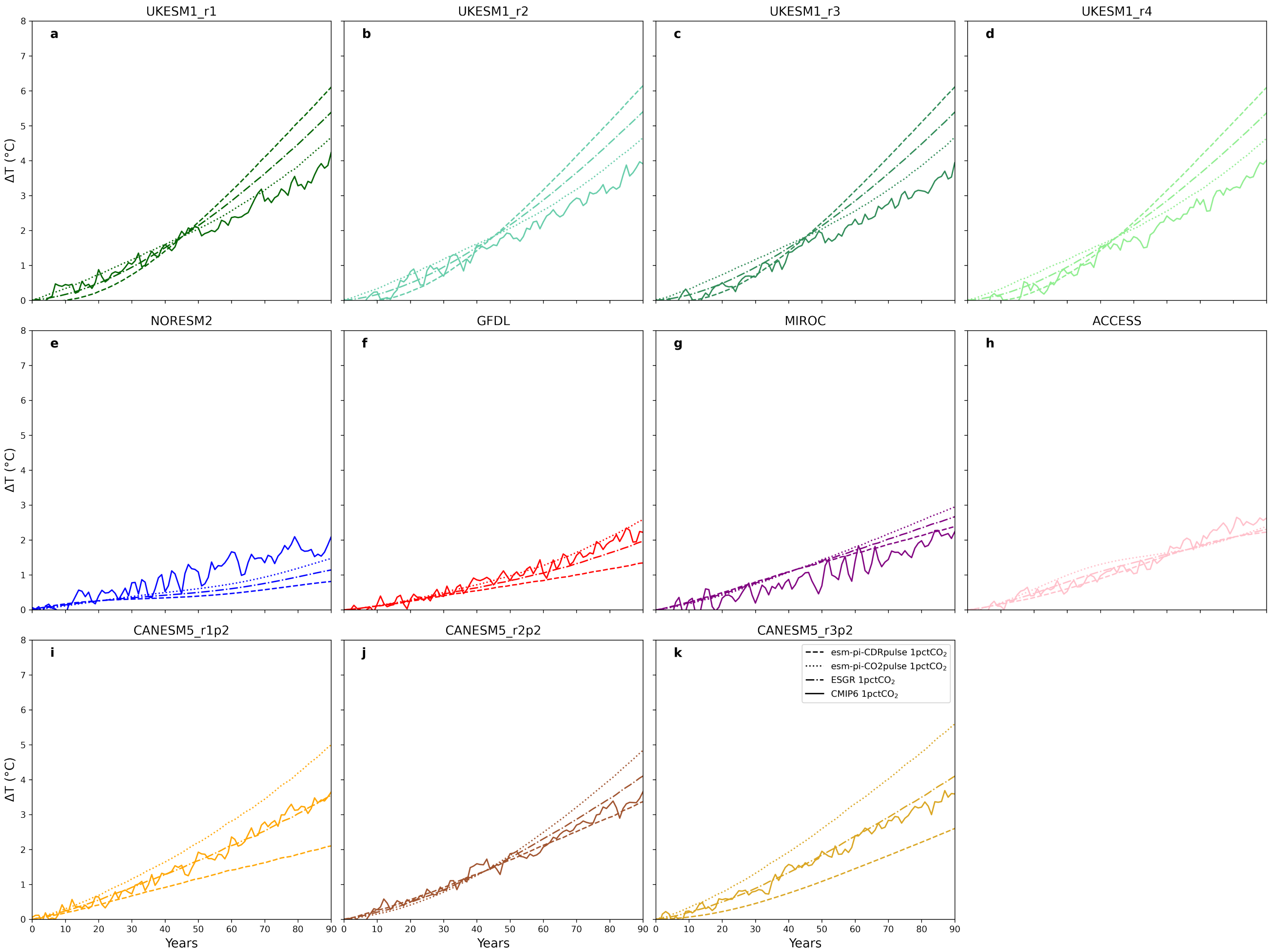

Figure S2. Global mean temperature change in each model for a *1pctCO*$_2$ experiment in the CMIP6 model, compared to ESGR and convolutions with the individual pulse types (*esm-pi-CO2pulse* and *esm-pi-CDRpulse*)

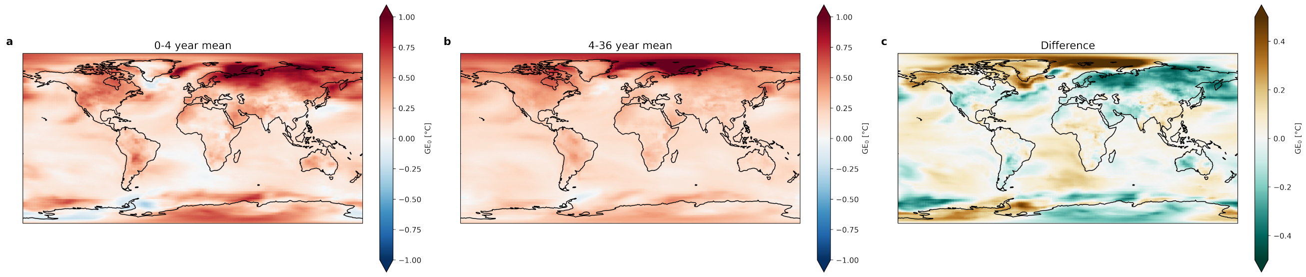

Figure S3. The time-mean ESGR scaled by the initial emissions size of 100GtC between 0-4 years and 4-36 years, and the difference between the two.

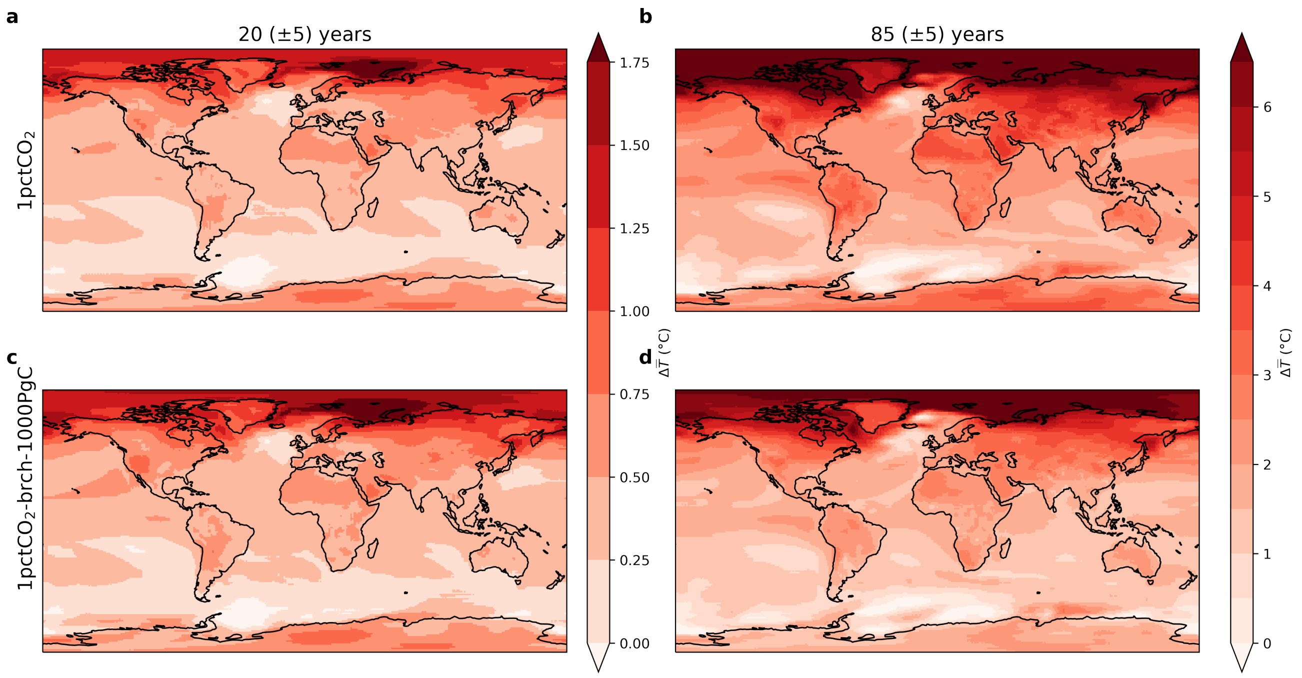

Figure S4. Temperature change in ESGR due to the *1pctCO*$_2$ and *esm-1pct-brch-1000PgC* scenarios at 20 ($\pm$5) years and 85 ($\pm$5) years.

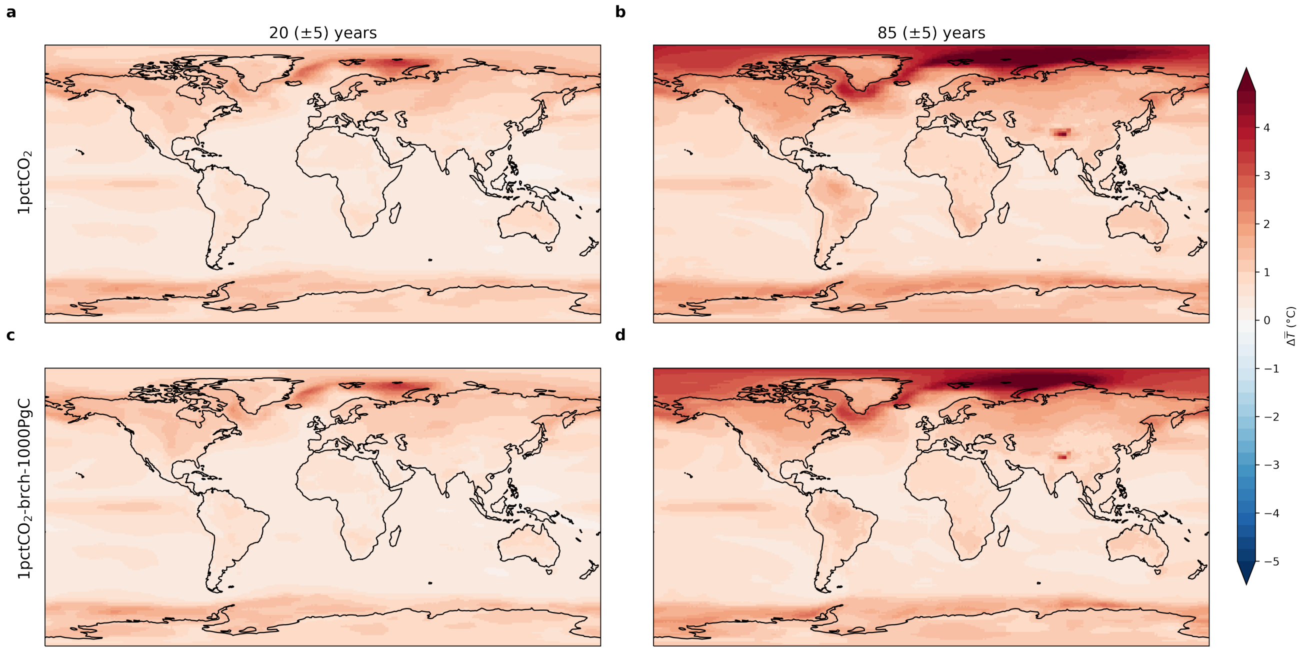

Figure S5. Intra model spread, shown as 1σ as used for determining hatching in S5 at 20 ($\pm$5) years and 85 ($\pm$5) years.

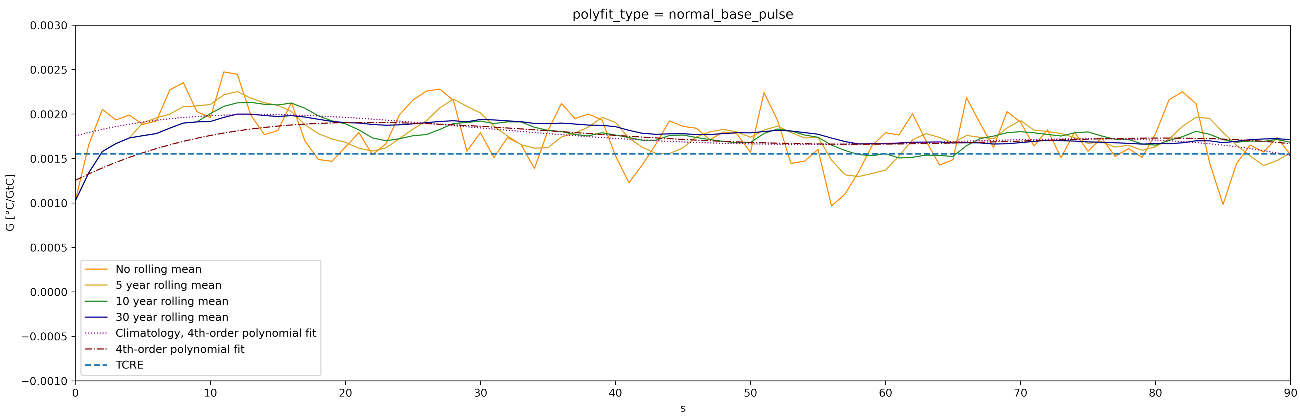

Figure S6. Global mean Green's function for the rolling mean at varying windows (5, 10, 30, and none), the 4th-order polynomial fit, and the 4th-order polynomial fit using a *pi-ctrl* climatology. The dashed line shows the TCRE.

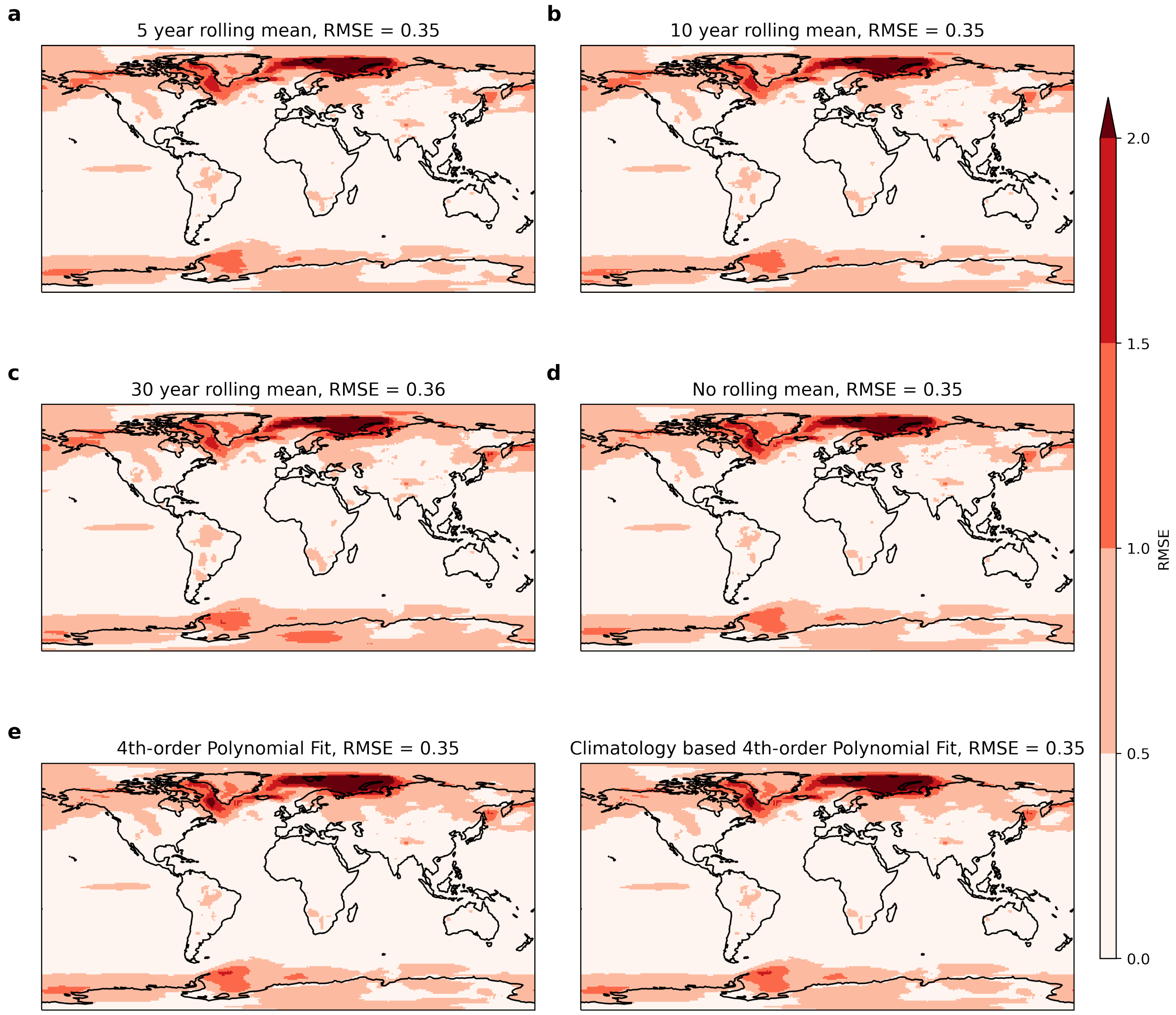

Figure S7. The root mean squared error (RMSE) for temperature change in ESGR compared to the CMIP6 *1pctCO*$_2$ multi-model mean. a) shows a 5-year rolling mean ESGR, b) a 10-year rolling mean, c) a 30-year rolling mean, d) no rolling mean, e) a 4th-order polynomial fit, and f) a 4th-order polynomial fit using the *pi-ctrl* climatology.

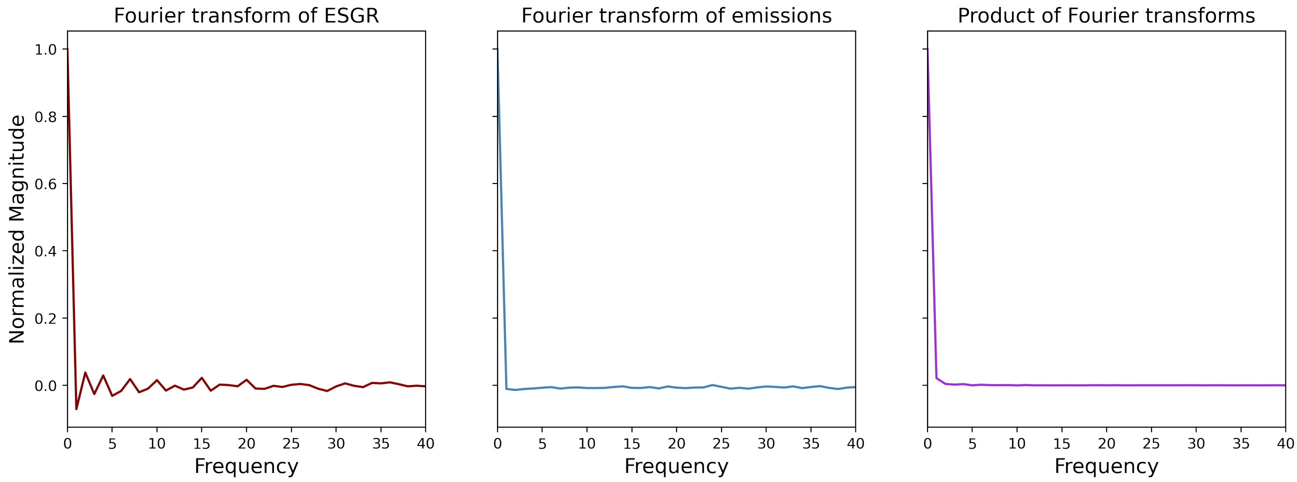

Figure S8. The Fourier transform of the global mean ESGR, the Fourier transform of the emissions from a multi-model mean *1pct-CO_2* experiment, and their product. All values are normalized to the peak magnitude.